X-622-65-436

NASA TM X-55392

RADIATIVE EQUILIBRIUM IN PLANETARY ATMOSPHERES II. AN ANALYSIS AND INTERPRETATION OF SOME VENUS OBSERVATIONS BASED ON A SINGLE REFLECTING CLOUD LAYER MODEL

BY

F. BARTKO

R. A. HANEL

SEPTEMBER 1965

NASA

GODDARD SPACE FLIGHT CENTER

GREENBELT, MARYLAND

Radiative Equilibrium in Planetary Atmospheres II. An Analysis and Interpretation of Some Venus Observations Based on a Single Reflecting Cloud Layer Model

by

F. Bartko
and
R. A. Hanel

Goddard Space Flight Center

Greenbelt, Maryland

September, 1965

SUMMARY

The equilibrium temperature distribution, thermal emission spectrum, and limb function of a nongrey N_2-CO_2-H_2O model atmosphere have been computed for a large variety of atmospheric parameters which are appropriate for the atmosphere of Venus in the vicinity of the cloud tops. Near infrared absorption by CO_2 of direct and diffusely reflected solar radiation as well as nonblack cloud emissivities have been included.

The important effects of the near infrared solar heating by CO_2 absorption, the water vapor amount, and the cloud top pressure level on the computed results are demonstrated. An application of this study to several observations of Venus yield the conclusion that atmospheric absorption by CO_2 cannot account for the limb darkening observed in the 8-13μ region. Other conclusions resulting from a study of the water vapor abundance and thermal emission spectrum depend on the cloud composition. If the clouds are ice crystals, their elevation is at the 0.2-0.4 atm pressure level. If their composition is nonaqueous, a pressure level of 0.4-0.5 atm may be assigned to the cloud tops. These results are based on the assumption of a single reflecting cloud layer, an assumed CO_2 concentration of 5% and a brightness temperature of 225°K for the cloud tops in the 8-13μ spectral interval.

Several observations are suggested in order to clarify the relative importance of the effects of various phenomena on the atmospheric and cloud structure of Venus.

Author

CONTENTS

LIST OF SYMBOLS

c_p - Specific heat (cal gm^{-1} $^oK^{-1}$).

d - Particle diameter (microns).

πF_a - Convective flux (watts cm^{-2}).

g - Gravitational acceleration on Venus (877 cm sec^{-2}).

h - Vertical distance (km).

H - Pressure scale height (km) (H_o = value at 273°K).

H* - Water vapor scale height (km).

i - Subscript denoting wavenumber interval.

- Mixing length (km).

m - Absorption coefficient defined by $\tau = (mu^*)^n$.

n - Exponent in computation of optical thickness.

P - Pressure (P_o = 1 atm).

q_{CO_2} - CO_2 volume concentration.

q_{H_2O} - H_2O volume concentration.

$q^s_{H_2O}$ - H_2O saturation volume concentration.

r_c - Cloud reflectivity.

S - Spectral line intensity (cm gm^{-1}).

T - Atmospheric temperature (T_o = 273°K).

t - Spectral line spacing (cm^{-1}).

u* - Modified pressure and temperature reduced path length (cm atm or gm/cm^2).

$\bar{v}$ - Mean gas velocity (cm sec^{-1}).

X - Parameter proportional to the product of the spectral line intensity and the ratio of the path length and line half width.

x - Distance from tropopause boundary (km).

LIST OF SYMBOLS (Continued)

α	-	Pressure broadened line half-width.
β'	-	Parameter proportional to the ratio of the spectral line half-width to the average line spacing.
β^*	-	Superadiabatic temperature gradient ($^oK\ km^{-1}$).
β	-	Adiabatic temperature gradient ($^oK\ km^{-1}$).
γ	-	Exponent describing temperature dependence of absorption by excited bands.
Γ	-	Ratio of specific heats, c_p/c_v.
$\epsilon_{\bar{\nu}c}$	-	Spectral emissivity of cloud surface.
ζ	-	Solar zenith angle.
η	-	Atmospheric viscosity.
μ	-	Direction cosine ($\mu = \cos\theta$).
$\bar{\nu}$	-	Wavenumber (cm^{-1}).
ρ	-	Atmospheric density ($gm\ cm^{-3}$).
ρ^*	-	Density of perturbed atmospheric element ($gm\ cm^{-3}$).
τ	-	Optical thickness.

I. INTRODUCTION

In a previous study, the authors (Reference 1) considered the structure of a planetary atmosphere in a state of radiative equilibrium. The radiative balance of a nitrogen-carbon dioxide atmosphere was determined to yield a number of temperature distributions. In that non-grey study, the absorption spectrum of CO_2 was divided into 18 intervals. Absorption coefficients were derived for each of these intervals from the calculations of Stull, Wyatt and Plass (Reference 2) and from the laboratory data of Burch, Gryvnak, Singleton, France and Williams (Reference 3). The strong line approximation (Reference 4, for example) was found to be valid for the range of pressures, temperatures, and concentrations under consideration. Furthermore, a plane parallel atmosphere consisting of 34 layers of constant mixing ratio, in local thermodynamic equilibrium was assumed. A lower surface with a specified temperature and emissivity and solar radiation incident from above completed the boundary conditions. Radiative balance was obtained by an iterative calculation on a digital computer.

A large number of solutions were found for various CO_2 concentrations, solar zenith angles, and cloud top temperatures, emissivities and pressures. Each solution yielded a temperature profile, the associated spectral intensities, and the limb functions.

The primary results of these studies, as applied to a portion of the Venus atmosphere, indicated that near-infrared absorption of solar radiation by CO_2 causes considerable atmospheric heating. Temperatures above the cloud layer may differ by as much as 70°K between the subsolar point and the night side. The cloud top pressure level also produced significant effects while the variation of the CO_2 concentration and the cloud top emissivity was less pronounced.

A number of new features were introduced into these calculations to improve and generalize their applicability. The changes were made desirable partly by the results obtained from that study and partly by new observational data.

Some previously obtained solutions showed large temperature gradients near the cloud top surface. In some cases, the adiabatic lapse rate was exceeded and, according to the Schwarzschild stability criterion, convective transport of energy would take place. A more realistic treatment should therefore include convection, and hence the calculations were modified to incorporate these effects.

In applying these calculations to the atmosphere of Venus, a second modification was found necessary, as a result of recent observations which confirmed the presence of water vapor. Hence, an analysis of absorption laws, similar to that carried out for CO_2, was applied to the water vapor spectrum and absorption coefficients were derived.

The final change concerns the method of obtaining the temperature distribution. This change is minor although it is expected to yield somewhat more accurate temperatures.

The above modifications permit a study of the following items:

1) The effects of water vapor on the equilibrium temperature profiles,
2) The effects of atmospheric parameters on the convective motions arising from convectively unstable solutions,
3) The dependence of the thermal emission spectra and the limb functions on the atmospheric parameters,
4) A synthesis of the above analysis into solutions which may be compared with planetary observations.

Before these items are illustrated, a brief discussion of the various modifications applied to the calculations will be presented.

II. NEW FEATURES OF THE CALCULATIONS

A. Water Vapor Absorption

The absorption spectrum of water vapor consists of three intervals of interest: the near infrared spectrum from 1 to 5μ with numerous bands, the 6.3μ band extending from 5 to 8μ, and the pure rotation band covering the interval from 10 to 1000μ.

For this analysis, the 6.3μ band is divided into two and the rotation band into 4 intervals as shown in Table I. Although the rotation band extends below 20μ and overlaps the CO_2 absorption, it is ignored in this range with only the CO_2 absorption taken into account. This simplification appears justified, since the optical thickness of H_2O in the 10-20μ region is at least one order of magnitude smaller than that of CO_2 for the concentrations expected on Venus. For the same reason, the near infrared absorption of H_2O was ignored.

Water vapor absorption data are required between 150-300°K and for the pressure range 1 to 10^{-3} atm. The absorption spectrum of water vapor has been studied in detail by a number of investigators. A convenient summary has been given by Goody (Reference 5).

TABLE I

Spectral Interval (cm^{-1})	2000-1600 1600-1100	500-333	333-250	250-200	200-0
Spectral Interval (μ)	5 -6.3 6.3-9.1	20-30	30-40	40-50	50-∞
$\bar{S}$ ($\frac{cm}{gm}$)	2.2×10^5	6.6×10^4	2.4×10^5	4.2×10^5	1.1×10^6
$\alpha_o(cm^{-1})$	0.10	0.09	0.09	0.09	0.09
$t(cm^{-1})$	1.0	2.0	2.0	2.0	2.0
β'_o	0.6	0.3	0.3	0.3	0.3
X(STP)+	3.1×10^3	1.0×10^3	3.8×10^3	6.6×10^3	1.7×10^4

+ computed for 9×10^{-3} gm/cm^2 of H_2O.

+ Requirement for strong line approximation : $X = \frac{2\pi Su}{\alpha} > 1.6$

Using fundamental data such as line widths, spacings and intensities, a check for the validity of the strong line approximation was carried out. This approximation was fitted to the data of Burch et al (Reference 3) for the 6.3μ band and the data of Palmer (Reference 6) for the rotation band using water vapor amounts from 10^{-3} to 10^{-2} gm/cm^2. The resulting coefficients m and n used in the expression for the optical thickness in the spectral interval i, $\tau_i = (m_i u_i^*)^{n_i}$, are summarized in Table II, along with an updated list of CO_2 coefficients. The temperature dependence of the populations of the rotational levels of the pure rotation band and of the vibrational level for the 6.3μ band was neglected. The pressure and temperature dependence of the line half-widths are included.

B. Vertical Distribution of Water Vapor

The calculations described in Part I (Reference 1) incorporate a constant mixing ratio for CO_2. Since CO_2 condensation appears to be unlikely, this procedure is justified. However, the relative ease with which water vapor may condense for the pressures and temperatures considered, makes it desirable to represent the vertical distribution of its concentration in a variable fashion. This may be accomplished by specifying the concentration as a function of pressure, for example, as shown in Eq. (1)

$$\log_e \left\{\frac{q(P)}{q_c}\right\} = \left(\frac{H-H^*}{H^*}\right) \log_e \frac{P}{P_c} \qquad (1)$$

The effects of a constant as well as a variable concentration will be discussed.

Table II - Absorption Coefficients

i	$\bar{\nu}$ (cm^{-1})	m	n	γ
1	0-200	2.6×10^{3}	0.35	0
2	200-250	8.0×10^{2}	0.40	0
3	250-335	1.7×10^{2}	0.38	0
4	335-495	1.2×10^{1}	0.35	0
5	495-550	7.8×10^{-5}	0.60	0
6	550-625	4.6×10^{-3}	0.42	0
7	625-660	9.0×10^{-1}	0.38	0
8	660-720	4.9×10^{-1}	0.42	0
9	720-810	9.5×10^{-4}	0.40	0
10	810-880	6.5×10^{-5}	0.55	2200
11	880-920	3.2×10^{-7}	0.47	2040
12	920-1000	7.5×10^{-6}	0.47	2040
13	1000-1100	1.6×10^{-5}	0.51	1950
14	1100-1600	2.5×10^{1}	0.44	0
15	1600-2000	1.0×10^{1}	0.45	0
16	2000-2600	6.6	0.50	0
17	2600-8000	1.1×10^{-3}	0.50	0
18	1700-8000(solar)	4.9×10^{-7}	0.27	0

u* - CO_2 in cm atm

u* - H_2O in gm/cm^2

C. Convective Effects

The results of Part I of this study showed in many cases a radiative gradient exceeding the adiabatic one, indicating a zone of instability. The radiative gradient is then not realized.

The criterion for stability as formulated by K. Schwarzschild (See References 7 and 8, for example) is expressed in terms of the adiabatic gradient, and the gradient actually maintained. The atmosphere is stable against convection if

$$(2) \qquad \left(\frac{dT}{dz}\right)_{actual} \leq \left(\frac{dT}{dz}\right)_{adiab} .$$

This criterion and the flux continuity condition yield the interface between zones of radiative and convective transfer. For a homogeneous atmosphere these conditions are equivalent to continuity of the temperature and the temperature gradient at the desired interface.

A modified form of Equation (2) was applied in the computer calculation using a method of successive approximations and taking the adiabatic profile as the initial temperature estimate. The atmosphere above a specific layer was permitted to adjust to radiative equilibrium to establish the gradient at this layer. Generally, 10 iterations were found to be sufficient. At the same time, the adiabatic profile was assumed to exist between this layer and the cloud surface. All layers contribute to the radiative solution although the constant flux criterion is applied only to the layers above the convective zone. In most cases, the normalized gradient will be highly positive at the starting layer indicating that the desired boundary must occur at higher pressures. As the next step, the interface is adjusted toward the cloud surface and the radiative solution established above this new layer. This process continues until the boundary conditions are satisfied within a predetermined tolerance. After finding the boundary location, the solution in the radiative zone is iterated until the net flux is constant over the whole radiative zone.

In addition to determining the tropopause height, the calculation permits an assessment of several other effects resulting from the convective transfer. At each point in the convective zone, the difference between the constant flux in the radiative regime and the radiative flux in the convective zone is the amount of energy transported by convection, πF_a.

In the atmosphere, this flux is produced by the vertical motion of mass elements, which may be written, neglecting geopotential and kinetic energies,

$$\pi F_a = \rho \bar{v} c_p T \quad . \tag{3}$$

In general, one half of the area element dA contains upward motion while the other half maintains downward motion, so that the net convective flux πF_a may then be expressed as

$$\pi F_a = \frac{1}{2} \rho \, c_p \bar{v} (\beta - \beta^*) \quad . \tag{4}$$

The quantity is a characteristic length, $\bar{v}$ is the average velocity of the moving element, and $(\beta-\beta^*)$ is the excess of the true gradient over the adiabatic gradient.

To obtain a further relationship among the parameters the equation of motion of the atmospheric elements may be integrated. The equation of motion is expressed as the balance of the buoyant and the inertial forces acting on the element:

$$\rho^* \frac{dv}{dt} = (\rho - \rho^*) \, g, \tag{5}$$

where ρ^* is the density of moving element, and ρ the density of the environment. At any given time, the convective motions may be considered as the superposition of periodic, closed path loops carried out by the moving elements. To a first approximation, Eq. (5) may be integrated to yield an average velocity $\bar{v}$,

$$\bar{v} = \frac{}{2} \left\{ \frac{g}{\Gamma T} (\beta - \beta^*) \right\}^{1/2} \quad . \tag{6}$$

The average vertical velocity and the excess gradient may be reformulated by combining Eqs. (4) and (6) with the adiabatic gas law, to yield

$$\bar{v}(h) = \frac{\Gamma - 1}{4\Gamma^2} \frac{g \quad (h) \pi F_a(h)}{p(h)}^{1/3} \quad \text{and} \tag{7}$$

(8) $$\frac{\beta - \beta^*}{\beta} = gH(\quad -1)^{1/3} \left(\frac{4 \quad \pi F_a}{p \quad 2} \right)^{2/3} .$$

The quantities $\bar{v}$ and β^* are expressed as functions of known quantities with the exception of the convective flux, πF_a, and the mixing length, .

The convective flux was obtained directly from the computer solution. The mixing length, , is more difficult to obtain. It may be defined as the characteristic length over which the linear momentum, ρv, is conserved, approximately. In a vertical column of gas the density ρ and the velocity $\bar{v}$ of the rising elements steadily diminish with height. Hence, an outflow of material must occur at the sides of the column. The distance over which

(9) $$\rho_2 \bar{v}_2 = \frac{1}{2} \rho_1 \bar{v}_1$$

is defined here as the mixing length and may be expressed more conveniently as

(10) $$\frac{1}{} = \frac{2}{\rho v} \frac{d(\rho v)}{dh} .$$

By an iterative process involving Equations (7) and (10) and the computed convective flux, the coefficients for a Taylor expansion of the mixing length are obtained,

(11) $$(h) = \frac{1}{2} x(h) - \frac{3}{8 \quad H} x^2(h) ,$$

where x is the distance from the tropopause and H the density scale height of an adiabatic atmosphere. The distance x is assumed to be small compared to the density scale height. The mixing length is slightly less than one half of the distance from a particular layer to the tropopause.

With this result, the superadiabatic gradient and the average vertical velocity may be computed. The gradient was found to exceed the adiabatic gradient by one degree per km at most, so that the use of the adiabatic profile in the computation appears justified. The desired vertical velocities were then computed using the mixing length according to Eq. (11).

One may then proceed a step further and determine the maximum particle size which could be supported by these velocities on the assumption of Stokes' law:

$$d = \left(\frac{18\eta \bar{v}}{\rho_p g}\right)^{1/2} \tag{12}$$

For the rough estimates of particle sizes presented later, more sophisticated forms of Stokes' law such as used in Ryan's study on Mars (Reference 9) are probably not warranted.

D. Temperature Calculation

The solution for the temperature distribution described previously (Reference 1) requires the specific temperature which balances the emission of each layer with its absorption. A relationship between the emission of a layer and its temperature was established by computing an array of values of emission, optical thickness, and temperature. When the absorption was computed, the value of emission identical to the absorption with the appropriate value of optical thickness was used to inspect the previously computed table for the value of temperature which satisfied the above conditions. This procedure sometimes yielded slightly different values of optical thickness in each side of the energy balance equation for those cases which showed very steep gradients.

A new approach was therefore adopted in which the value of optical thickness for a layer, based on the previously iterated temperature distribution is used in the emission as well as the absorption term, thus eliminating the small discrepancy.

III. EFFECTS OF INDIVIDUAL PARAMETERS

The maximum number of parameters used in any analysis is determined by the ability to represent the physical situation and by the number of independent observational data which are available for interpretation. For this study of the Venus atmosphere, the following parameters were selected.

Cloud Top Pressure	-	P_c
Cloud Top Temperature	-	T_c
Cloud Top Spectral Emissivity	-	ϵ_{ic}
Cloud Top Reflectivity (near infrared, 1-5μ)	-	r_c
Carbon Dioxide Concentration	-	q_{CO_2}
Water Vapor Concentration	-	q_{H_2O}
Solar Zenith Angle	-	ζ

The effects of a variation of specified combinations of these parameters may be studied on temperature distributions, thermal emission spectra, and limb functions. In the following discussions, the effects of the above parameters on each of these results will be presented separately.

A. Effects on Temperature Distribution

The results of a previous parametric analysis (Reference 1) applied to the equilibrium temperature distributions are summarized in Figures 1 and 2. In Figure 1, the strong effect of the near-infrared solar heating is evident from the change of temperatures with the solar zenith angle. The large temperature differences found between night and day are understood by a larger solar constant, a relatively high CO_2 concentration, and a high cloud top reflectivity.

Figure 2 illustrates the influence of the CO_2 concentration on the equilibrium temperatures for two cloud top pressures. The CO_2 effects differ somewhat for night and day. On the night side temperatures depend little on the CO_2 concentration, except in the uppermost layers, which are able to cool more effectively for the higher CO_2 concentrations. The illuminated hemisphere shows larger effects, especially near the cloud surface where the opacity for solar radiation is greatest, thus increasing the solar heating in these layers for higher CO_2 amounts. The strong influence of the cloud top pressure is also evident.

The influence of the cloud top emissivity on the temperature distributions is not illustrated. An emissivity of 0.8 showed negligible influence on the shape of the equilibrium temperature distributions. Similarly, a 10% variation in the adopted value of 0.6 for the near infrared cloud top reflectivity shows a minor effect and is not shown.

Water vapor influences the equilibrium temperatures distinctly. This is shown in Figure 3 for a cloud top pressure of 0.3 atm, for noon and night conditions. Several concentrations and their respective saturation curves (Reference 10) are illustrated.

Also shown for the same total amounts of H_2O under noon time conditions, are two additional temperature distributions using water vapor scale heights of 1/3 and 2/3 the pressure scale height. Such variations allow an effective balance of H_2O cooling and CO_2 heating, yielding a nearly isothermal atmosphere. At the same time, the temperature distribution in the upper regions depart further away from the saturation curves. Tropopause heights are also indicated, when they appear.

The effects of water vapor on the equilibrium temperature distributions may be summarized as follows.

1. Large amounts of water vapor introduce substantial cooling of the sunlight hemisphere. This is understood from the atmospheric opacity in the rotational band, where approximately one-half of the energy spectrum lies..

2. A growth in the convective zone results with the addition of water. Again, the cooling influence of water vapor increases the radiative gradient and the convective flux, thus extending the zone to greater altitudes.

3. The condensation properties of water vapor coupled with the convective instability imply that the night side cloud tops would grow to higher altitudes than the day time clouds, other parameters being held constant. On the illuminated hemisphere condensation may or may not take place depending on the water vapor concentration and its vertical distribution. In either hemisphere, the latent heat released or absorbed in the vapor-ice phase transitions would yield a substantial influence on the resulting cloud top temperature as well as the vertical distribution adjacent to the cloud tops.

As discussed previously, an assessment of the effect of the atmospheric parameter on the relevant quantities of the convective motion is possible. The dependence of the tropopause height, the magnitude and the vertical distribution of the convective flux, and the associated vertical gas velocities may be studied. Figure 4 shows each of these items for one particular combination of atmospheric parameters.

The situation illustrated is for an 0.3 atm cloud top pressure level under night time conditions and unit emissivity. The convective flux, the mixing length, the mean vertical velocity, and maximum particle size are shown as a function of the distance

from the tropopause. In all cases studied the convective flux increased with the square of the distance from the tropopause. Since the analysis is based upon a mixing length theory and other simplifications, the results for the mean velocities and particle sizes are only approximate.

A study of several sets of computations shows that the magnitude of the convective flux increases as the cloud top pressure is increased, primarily as a result of the increased atmospheric density. The corresponding mean vertical velocities and maximum particle diameter decrease in magnitude, however.

C. Effects on Thermal Emission Spectra

The effects of the atmospheric parameters on the thermal emission spectra will now be discussed. The most influential parameter is the solar radiation. For the case illustrated in Figure 5 where the brightness temperature is plotted as a function of wavenumber, with the wavenumber scale arranged in equal energy increments for a 225°K blackbody, solar heating reverts the 15μ CO_2 band from pure absorption to a partially absorption and partially emission spectrum. The most dominant feature is the 15μ CO_2 band, although the rotation band of H_2O appears moderately strong. The 8-13μ region appears rather uniform, except for subsolar conditions where the temperature dependence of the CO_2 bands, combined with a large temperature inversion produce moderate features.

The effect of cloud top pressure is also pronounced (Figure 6). For low pressures, very little structure appears in the spectrum, due to the small total opacity of the atmosphere. At higher pressures spectral features stand out strongly, even for small CO_2 concentrations. Figure 7 shows the effects of varying the CO_2 concentration under night time conditions. As expected, the spectral features become more intense as the opacity of the atmosphere increases.

The effects of cloud top emissivity are shown in Figure 8. For this study, the emissivity beyond 13μ was taken as unity but was permitted to assume some specified value at shorter wavelengths. The combination of surface temperature and emissivity was adjusted to maintain about 225°K, close to the observed value of the brightness temperature in the atmospheric window. The effects in the 15μ band and the rotational band are moderate. A small increase in the surface temperature with a constant emissivity elevates the entire spectrum, keeping the shape of the spectrum essentially intact.

Figure 9 illustrates the effects of varying the H_2O concentration. The primary influence appears in the rotational band for large concentrations.

C. Effects on the Limb Functions

The computed limb functions allow further studies of the model atmospheres. The limb functions depend primarily on the optical thickness of the atmosphere. In the absence of strong scattering effects, the variations in the limb function depend on the temperature variations over the surfaces of constant optical thickness.

Two of the eighteen spectral intervals are illustrated in Figure 10. These are the 1064 cm^{-1} band and the 625-640 cm^{-1} region and they represent weakly and strongly absorbing intervals, respectively. The limb function variation is determined by the magnitude of the temperature inversion, and therefore by solar heating, and the opacity of the spectral interval. The effect of solar heating on the weak interval is well illustrated while the CO_2 influence is shown best by the strongly absorbing interval.

Figure 11 shows the effect of cloud top pressure on the limb functions, the variations being larger for the weakly (495-550 cm^{-1}) absorbing interval. The H_2O variation is small, although a slight reversal of the pressure effect is seen in the strongly absorbing interval (625-660 cm^{-1}) in Figure 11. The effect of varying the cloud top emissivity is negligible for the intervals discussed and is not illustrated.

IV. APPLICATION OF RESULTS TO A COMPARISON WITH SOME VENUS OBSERVATIONS

Several observations are available which may provide a test of these calculations. These are considered in the following order:

A. Various observations relating to the presence of water vapor. (References 11, 12, 13, 14, 15, 16, 17)

B. Limb function observations in the 8-13μ interval by Sinton and Strong (Reference 18), by Sinton (Reference 19) and the more recent thermal maps obtained by Murray, Wildey, and Westphal (Reference 20).

C. The thermal emission spectra measured in the 8-13μ interval by Sinton and Strong (Reference 18).

A. Water Vapor Measurements

A knowledge of the presence of water vapor in the Venus atmosphere is very significant. In moderate to large amounts, water influences the atmospheric structure from a radiative as well as a dynamical point of view. The question of cloud composition is also associated with the presence of water in the vapor state. Finally, the presence of water is an important indication of the historical development of the planet and its atmosphere. The discussion presented here will only be concerned with the influence of water vapor on the atmospheric structure and its relation to cloud phenomena.

The existence of water vapor in the Venus atmosphere was first suggested by Strong et al's 1959 balloon measurements (Reference 21). These were repeated in 1964 with improved apparatus and again yielded positive results (Reference 13). Similar measurements by Dollfus (Reference 17) using the 1.38μ region were also positive. In both cases the actual quantities of water vapor deduced require considerable interpretation since the values depend heavily on the pressure level of the reflecting layer. On the other hand, Spinrad's (Reference 11) spectroscopic analysis of the .87μ bands has produced 10^{-6} for the mass mixing ratio, a value leading to amounts below Bottema et al's and Dollfus's amounts, unless the reflecting cloud layer is placed at relatively high pressures (>1 atm).

Another observation indicating the presence of water vapor is the more recent balloon measurements of Bottema, Plummer, Strong, and Zander (Reference 14) which have shown that the reflectivity of the cloud layer in the Venus atmosphere to be similar to that of ice crystals. Nevertheless, high resolution spectra obtained by Kuiper (Reference 15) and by Moroz (Reference 16) near 2μ do not reveal the characteristic ice crystal absorption. No attempt will be made at reconciling these results; instead an analysis presenting both viewpoints will be considered and illustrated here.

Since the deduced amounts of water vapor depend strongly on the cloud top pressure level, the limits usually quoted for this level in the literature (Reference 22, for example) (0.09 -0.60 atm) will be illustrated. Table III summarizes the water vapor concentrations deduced for each pressure level, for two of the investigations cited. The results of the calculations using the values listed in Table III are illustrated in Figures 12, 13 and 14.

TABLE III - H_2O CONCENTRATIONS

Reflecting Layer Pressure Level	0.09 atm.	0.60 atm.
Spinrad(1963) Volume Concentration	1.6×10^{-6}	1.6×10^{-6}
Bottema et al (1965) Volume Concentration	4.2×10^{-3}	6.7×10^{-6}
Saturation Volume Concentration	5.6×10^{-4}	8.3×10^{-5}

Consider first a cloud layer consisting of ice crystals. Under these conditions, the observed amount of water must provide saturation at the cloud top. For 0.09 atm (Figure 12) and a cloud top emissivity of unity, the large degree of cooling generated by the emission in the H_2O rotational band offsets the solar heating due to near infrared absorption by CO_2. Comparison with the condensation curve implies a super-saturated atmosphere even under noon-time conditions and hence is incompatible with this pressure level. On the night side, the condensation coupled with convective motions would elevate the cloud top to higher altitudes.

In Figure 13, the reflecting cloud layer is placed at 0.60 atm and the results show that the solar heating produced by the near infrared absorption of CO_2 dominates the H_2O cooling. The temperature distributions do not allow saturation at this pressure level. Hence, the cloud layer, if composed of ice, must be placed at a higher elevation, until saturation is possible at the cloud tops. This occurs at approximately 0.30 atm, although a more definite level is not offered since the absorption law (1.13μ band) is intermediate between weak and strong for this pressure range and water amount. This interpretation implies that the observed water pertains essentially to the clear atmosphere above the clouds and not to deeper layers.

The above analysis may represent an over-simplified interpretation since other atmospheric conditions are capable of providing alternative points of view which might still be consistent with the 0.09 atm level. Among these possible conditions are:

1. The cloud top emissivity may be less than unity and therefore the true temperature in the vicinity of the cloud tops may be higher than the observed brightness temperature of about 225^{o}K. Cloud emissivities near unity are characteristic of thick water or ice crystal clouds. Lower values of emissivity correspond to either nonaqueous or semi-transparent cirrus-type clouds. The reduced apparent brightness temperature which results in such cases corresponds to higher values of true cloud top temperature. The corresponding equilibrium temperature distributions may then be shifted beyond the saturation curves and condensation thus avoided.

The calculations using a cloud emissivity of 0.5 with a cloud top temperature of 255^{o}K placed at 0.09 atm is shown in Figure 14. Condensation would again occur, and since 0.5 is probably a lower realistic limit for the cloud emissivity, this pressure level may be rejected.

2. The H_2O measurements may have actually "penetrated" through the clouds to deeper layers, so that the water vapor concentrations shown in Table III should be considered upper limits. If water amounts which could avoid condensation are desired, then the observation would be required to penetrate one or two scale heights into or below the clouds. Although this requirement is rather severe for a single reflecting cloud layer, it is difficult to reject categorically.

3. The water vapor may exist in a nonuniform vertical distribution in which case the total amount of H_2O deduced would be modified. Also shown in Figures 12 and 14 are temperatures computed with a very nonuniform vertical H_2O distribution, keeping the total amount the same as in the uniform distribution case. For a cloud emissivity of unity, the previous conclusions are not significantly altered. If the cloud emissivity is about 0.5, then condensation for noon time conditions could be partially avoided, although larger solar zenith angles would still exhibit condensation. Again, this constraint on water clouds is severe, and the vertical distribution used rather extreme. Condensation appears to be difficult to avoid. Hence, the third alternative may be discarded. The net conclusion of this part of the analysis, with some reservation, is that the reflecting ice crystal cloud layer should exist at the 0.20-0.40 atm pressure level with an assumed cloud top temperature of 225°K.

A similar analysis may now be considered for nonaqueous clouds. In this case, the atmosphere must everywhere lie well below saturation. A typical value that may be considered for the mass mixing ratio of water vapor is Spinrad's value of 10^{-6}. For an emissivity of unity, condensation is not possible under daytime conditions for either the 0.09 or 0.60 atm cases as shown in Figures 12 and 13. For both pressure levels, condensation and cloud formation would be likely on the dark hemisphere although an emissivity as low as 0.5 may restrict the condensation on the night side to thin haze layers in the upper regions. Concentrations less than 10^{-8} or emissivities of about one-half would be necessary to avoid H_2O clouds entirely on the night side. Either requirement would be consistent with nonaqueous clouds for most pressure levels. However, two limits on the cloud top pressure may be derived on the assumption of nonaqueous clouds. If a total water content of 9×10^{-3} gm/cm^2 (Bottema et al)(Reference 13) is assumed to exist above the clouds, with a cloud top temperature of 225°K, then cloud top pressures in excess of 0.4 atm are required to avoid saturation at the cloud tops. An upper limit may be determined with Spinrad's mixing ratio of 10^{-6}. An examination of Figure 13 reveals that a temperature of 225°K is not achieved with the

saturation curve for pressures less than 1 atmosphere. In fact, a pressure of 31 atmospheres is necessary to reach a temperature of 225°K. If lower emissivities and higher temperatures are appropriate, then this pressure range would be shifted to higher values. Further conclusions on the cloud level and other atmospheric parameters will be considered in the subsequent sections dealing with other observations.

B. Limb Function Observations

The detailed thermal maps produced by Murray, Wildey and Westphal (Reference 20) and the limb functions obtained by Sinton and Strong (Reference 18) and by Sinton (Reference 19) provide another set of observational data to compare with the computed results. The latter measurements indicate a darkening proportional to the square root of the view angle cosine, while Murray et al's data show a somewhat weaker dependence.

The results are compared in Figure 15 in which the partially illuminated hemisphere is observed to yield a darkening not generally different from the night side of the planet. However, the calculations using intensities averaged over the six spectral intervals comprising this portion of the spectrum indicate a substantial brightening in the illuminated hemisphere. The illuminated hemisphere is represented by a composite of two zones, whose average solar zenith angles are 60° and 75°. These two zones used in conjunction with a dark side computation are sufficient to represent the planetary phase during the observations of Murray et al. Three situations are compared with the observed result. The light solid curve results from a calculation placing the cloud tops at 1.0 atm. The dashed and dotted curves result from an 0.3 atm pressure level under various assumptions. The dashed case results from differences in the computed temperature distributions over the disk and show little variation with some asymmetry in the limb function, while the 1.0 atm case shows appreciable night side darkening with considerable asymmetry. The dotted case is discussed later. A darkening comparable to the observed amount can be obtained with a more opaque atmosphere (P_c > 1 atm). Such an opaque atmosphere, however, yields an even greater degree of brightening on the illuminated hemisphere, which is enhanced and the asymmetry increased in the computed limb functions as the planetary phase is increased. Sinton's observations clearly illustrate that little change, if any, occurs in the shape of the limb function under various phase angles. Hence, the solar heating and its related brightening must be minimized or its effects eliminated to yield accordance with the observations since an explanation of the observed darkening cannot be made on the basis of an absorbing atmosphere alone. The disparity between the observations and calculations suggest the following considerations as means for reconcilation.

1. A very low CO_2 concentration ($q_{CO_2} << 0.05$) may be necessary to minimize the effects of solar heating and its subsequent contribution to the limb brightening. However, such low concentrations, whatever their value, must still be capable of yielding the observed equivalent widths of the CO_2 bands in the red and near infrared portions of the spectrum. Moreover, the atmosphere becomes so transparent, unless large values of cloud top pressures are used, that the requisite absorption is not available to yield the darkening function.

2. The clouds may be responsible for the observed limb darkening. Scattering by cloud particles, a large negative temperature gradient within the cloud, the vertical cloud structure, or some combination of these items may contribute to the observed limb darkening. A number of authors have considered these possibilities (References 23, 24,25,26 and 27 for example) and have demonstrated that each is capable, alone or with some realistic combination, of explaining the observed darkening.

3. If larger CO_2 amounts do exist, then the computed brightening in the sunlit hemisphere may be removed by dynamical processes. Global convection currents giving rise to adiabatic cooling in the sunlit hemisphere and an adiabatic heating on the night side could yield approximately the same temperature distribution above the clouds for day and night conditions. Solar heating may be sufficient to act as a driving force for a general atmospheric circulation. The maximum effects permitted by such a circulation, with the observed amounts of H_2O, would yield a temperature distribution somewhat above the corresponding saturation curve for H_2O. Although this distribution is rather arbitrary, it is a convenient and physically plausible one to use. The net result of such circulation may be simulated with these computations and the result is shown as the dotted curve in Figure 15. The degree of darkening still falls short of the required amounts. High pressures, coupled with such circulation would be required, but saturation cannot be achieved at these levels with the observed amounts of H_2O.

The conclusions from this part of the analysis hinge on the presence of several possible physical conditions or phenomena. If the clouds consist of ice crystals then somewhat lower CO_2 concentrations, scattering by the cloud particles, or atmospheric motions to remove the solar heating effects, or a proper combination of all three items are required to yield the observed darkening.

If the clouds are not water vapor, then even lower CO_2 concentrations would be necessary to reduce the solar heating, but then the observed darkening becomes more difficult to achieve on the night side. The net result remains the same, in either case, that the clouds must be responsible for producing the observed limb darkening.

C. Thermal Emission Spectrum of Sinton and Strong

Measurements of the emission spectrum of the planet Venus were reported by Sinton and Strong in 1960 (Reference 18). The total disk of the planet was used to record the spectrum from 8-13μ. In order to simulate this observation with these calculations, the planet was divided into several zones of varying solar zenith angle. In addition, identical zones of aspect or view angle, rotated ninety degrees from the zenith angle zones toward the observer, are superposed on the planet. The resulting grid is shown in Figure 16, where the mean solar zenith angle and mean aspect angles for each zone are indicated. Symmetry permits consideration of only one half the observed hemisphere. The computed spectra were synthesized by taking the specific intensity from each of the six areas and weighting the values by the relative projected area of each zone. These are then summed to yield a flux value emitted by the illuminated hemisphere. This is repeated for each spectral interval over the range 8-13μ, using intervals 40-100 cm^{-1} wide. These fluxes are then averaged with their corresponding spectral fluxes from the night hemisphere to yield the final value. A refinement of the procedure using greater spatial resolution yielded no significant differences.

Ideally, a comparison yielding agreement of the computed spectra with the observed one, is desirable over the whole 8-13μ interval. At best however, only a qualitative agreement could be achieved in two ways. The overall shape of the spectrum, neglecting the 11.2μ feature can be reasonably computed. Alternatively, a comparison can also be attained on the basis of the 11.2μ feature alone. Several combinations of atmospheric parameters were considered and synthesized, and are shown in Figures 17 and 18, where the brightness temperature is plotted as a function of wavelength. The effect of cloud top pressure is shown in Figure 17, assuming a cloud top emissivity of unity. The overall shape of the spectrum is fairly well reproduced, although as may be expected, no feature at 11.2μ is apparent. A slight increase of cloud top temperature will increase the general level of the spectrum to yield a better agreement, without altering its shape. It may be noted that an increase in the pressure level yields colder temperatures in the 12-13μ region. All three pressure levels appear to yield fair agreement.

Figure 18 illustrates an attempt at duplicating the 11.2μ feature, without the presence of an additional atmospheric absorber or a peculiar cloud top spectral emissivity. A cloud top emissivity of one-half is shown for several pressure levels. Good agreement in the 10-13μ region is obtained with a cloud top pressure of 0.3-0.5 atm. Again, the general level may be increased to improve the match by a slight increase in cloud top temperature without destroying the shape. Emissivities smaller than 0.5 yield excessively high temperatures in the 8-10μ region while values larger than 0.7 are insufficient to yield the 11μ feature, which originates from a combination of the transparency of this spectral interval and the decreased emissivity. The 0.3-0.5 atm pressure level appears to yield the best fit for this portion of the spectrum.

At this point it may be mentioned that a more detailed or extensive study is not justified until more observational studies confirm the spectrum and its 11.2μ feature, preferably under varying spectral resolution, if possible. Pending such confirmation, however, it is felt that the general trends introduced into the spectra by various factors are still of interest and may contribute to the number of qualitative deductions permitted by such an analysis.

A factor necessary to consider is the influence of the observed limb darkening on the spectra. This effect may be considered by applying the observed limb function to the synthesized spectra, such that the contribution from the outer zones of aspect angle is reduced. In effect, the weighting factors for the outer zones were decreased according to the observed limb darkening. Discernable differences of spectra computed with and without this alteration were not found.

A second factor which influences the spectra is the presence or absence of solar heating on the sunlit side of the planet arising from near infrared CO_2 absorption in the atmosphere. If radiative equilibrium alone prevails then the sunlit side of the planet should be warmer than the night side and the resulting spectra are those shown in Figures 17 and 18. If, however, planetary convection predominates over the radiative equilibrium, nearly uniform temperatures may be expected on the day and night sides of the planet and result in correspondingly different spectra. This result may be simulated in the computed spectra by examining the spectra resulting from the use of a single temperature distribution over the planet. An arbitrary but physically reasonable temperature distribution to use under such assumptions in the presence of water vapor, would be the saturation curve corresponding to the observed amount of water. An examination of the spectra resulting from the use of the H_2O saturation curves as the temperature distribution in both hemispheres yields a flat blackbody

spectrum of about 225°K in the 8-13μ region. The use of a steeper gradient gives nearly identical results, with only a slight drop in the 12-13μ temperatures. Hence, a composite spectrum as shown in Figures 17 and 18, which includes the differences in the day and night hemispheres, appears to be necessary to yield a close agreement in the overall shape of the spectrum.

The effect of the accuracy of the absorption coefficients may also be discussed presently. A study showed that a 20% change in the coefficients yielded no significant difference in the shape of the computed spectra.

Further conclusions based on a spectral comparison alone, require a discussion of the cloud composition. Cloud emissivities near unity, which are characteristic of opaque ice crystal clouds, are capable of yielding computed spectra in fair agreement with the general shape of the observed spectrum, using a cloud top pressure in the range 0.1-0.3 atm. The 11.2μ feature is not apparent under these conditions. On the other hand, cloud emissivities in the range 0.5-0.7 correspond to nonaqueous clouds and provide computed spectra yielding the 11μ feature, but with somewhat poorer agreement in the 8-9μ interval, using cloud top pressures from 0.3-0.5 atm. Spectral emissivities peculiar to other cloud substances, in combination with the other atmospheric parameters cannot be ruled out, and may yield better agreement. An interesting possibility is a combination of ice crystallized onto particles of $CaCO_3$ or Na_2CO_3. Either of the latter two substances show strong features at 11.2μ and may be possible cloud particle candidates (Reference 28, 29).

These conclusions are at best qualitative and suggestive only. A factor not considered here which may play as great a role in determining the observed spectrum as the composition, is the vertical cloud structure. Further analysis must await repeated observation of the spectrum, preferably carried out over various portions of the disk, isolating the sunlit and dark hemispheres, if possible.

V. SUMMARY AND CONCLUSIONS

An attempt has been made to illustrate the important effects of several parameters on the atmospheric structure in the Venus atmosphere above the cloud layer. The results indicate that the cloud top pressure, water content and solar heating by CO_2 absorption have a strong influence on the atmospheric structure. A comparison of these calculations with several observational data provides a severe test.

Within the limitations of the calculations and the assumption of a 225°K brightness temperature for the cloud tops and a 5% CO_2 concentration, the results of such a comparison lead to the following conclusions:

1. A study of the water vapor abundance yields a cloud top pressure of ~0.3 atm for ice crystal clouds, and pressures greater than 0.4 atm for nonaqueous clouds.

2. Studies of the thermal emission spectrum show good agreement with the observations, over the pressure range, 0.1-0.8 atm, for unit cloud emissivities and 0.3-0.5 atm for smaller emissivities (~0.5).

3. The limitations on the cloud top pressure level may be further restricted by merging the above results. A pressure range of 0.2-0.4 atm appears most probable for ice crystal clouds while values from 0.4-0.5 atm appear reasonable for nonaqueous clouds. These limitations on the cloud top pressure are based on a constant spectral emissivity. However, the clouds themselves may be totally responsible for the observed spectrum, in which case the use of an appropriate, variable spectral emissivity would probably yield some adjustment in these limitations.

4. An analysis of the limb function calculations yields no further limitations on the cloud top pressure but yields the conclusion that the clouds are responsible for the observed limb darkening. Earlier studies, not considered here, of the planetary heat balance yielded similar inconclusive results for the cloud top pressure, within the limits of the observed albedo.

In order to improve the precision of the results and to clarify the importance of various atmospheric phenomena and other factors, the following observations are suggested.

a. A continuation of the detailed thermal mapping as a function of planetary phase.

b. A repetition of the 8-13μ spectrum using distinctly sunlit or night portions instead of the total planet.

c. If possible, measurements of the total thermal spectrum including the 15μ CO_2 band, again resolving day or night portions of the planet.

d. Ground-based measurements of the near IR CO_2 bands would also be desirable as a function of solar zenith angle over the planet.

e. High spatial and spectral resolution studies of the photographic IR spectrum of Venus. Possible variations with time and position over the sunlit disk of the planet, as a function of phase, are needed to provide a better physical picture of the cloud structure, as well as a clearer indication of the relative roles of scattering and absorption. High resolution spectra with the slit placed over various zones of equal solar zenith angle may provide some indication of variations in the rotational temperature over the sunlit part of the disk. Similar spectra with the slit adjusted perpendicular to the terminator may yield some data on variations in the cloud top elevation with solar zenith angle, if present.

As may be seen from the above conclusions, the incomplete agreement of the calculations with certain observations suggests that the simple reflecting cloud layer model may be inadequate. Hence, further theoretical studies in developing more realistic cloud models and their subsequent influence on the atmospheric structure are needed.

ACKNOWLEDGEMENT

The authors would like to express their appreciation to Mr. A. F. Simmons for his continued excellent programming efforts, and to Mr. W. R. Bandeen for a critical reading of the manuscript.

REFERENCES

1. Hanel, R. A. and Bartko, F., 1964 : Radiative Equilibrium in Planetary Atmospheres, I: Application of the Strong Line Absorption Law to the Atmosphere of Venus. NASA TN D-2397, Washington, D. C.

2. Stull, V. R., Wyatt, P. J., and Plass, G. N., "The Infrared Absorption of Carbon Dioxide," Air Force Systems Command, Los Angeles, California, Report SSD-TDR-62-127, V. III, January, 1963.

3. Burch, D. E., Gryvnak, D., Singleton, E. B., France, W. B. and Williams, D., 1962. Infrared Absorption by Carbon Dioxide, Water Vapor and Minor Atmospheric Constituents. AFCRL-62-698.

4. Plass, G. N., "Useful Representations for Measurements of Spectral Band Absorption," J. Opt. Soc. Amer. 50(9): 868-875, September, 1960.

5. Goody, R. M., 1964 : Atmospheric Radiation, Vol. 1, Oxford, Clarendon Press.

6. Palmer, C. H., 1960 : Experimental Transmission Functions for the Pure Rotation Band of Water Vapor, J. Opt. Soc. Amer., 50, p. 1232.

7. Schwarzschild, M., 1958 : The Structure and Evolution of Stars. Princeton University Press, Princeton, N. J.

8. Wasiutynski, J., 1946 : Studies in Hydrodynamics and Structure of Stars and Planets. Astrophysica Norvegica, Vol. 4, 497 pp.

9. Ryan, J. A., 1964 : "Notes on the Martian Yellow Clouds" J. of Geophys. Res., Vol. 69, p. 3759.

10. Smithsonian Physical Tables, 1956, 9th Revised Ed., Washington, D. C.

11. Spinrad, H., "A Search for Water Vapor and Trace Constituents in the Venus Atmosphere," Icarus 1(3); 266-270, October, 1962.

12. Bottema, M., Plummer, W., and Strong, J., 1964 : Water Vapor in the Atmosphere of Venus, Astrophys. J., Vol. 139, p. 1021.

REFERENCES (Continued)

13. Bottema, M., Plummer, W., and Strong, J., 1965 : A Quantitative Measurement of Water Vapor in the Atmosphere of Venus. Annales d'Astrophysique, Vol. 28, p. 225.

14. Bottema, M., Plummer, W., Strong, J., and Zander, R., 1964 : The Composition of the Clouds of Venus. Astrophys. J., Vol. 140, p. 1640.

15. Kuiper, G. P., 1963 : Infrared Spectra of Stars and Planets, I: Photometry of the Infrared Spectrum of Venus, 1-2.5μ. Communications of the Lunar and Planetary Laboratory, U. of Arizona, Vol. 1, #15.

16. Moroz, V. I., "The Infrared Spectrum of Venus (1-2.5μ)," Sov. Astronom. AJ 7(1):109-115, July-August, 1963.

17. Dollfus, A., "Observations of Water Vapor on the Planet Venus," C. R. Acad. Sci. 256(15):3250-3253, April, 1963.

18. Sinton, W. M., and Strong, J., "Radiometric Observations of Venus," Astrophys. J. 131(2):470-490, March, 1960.

19. Sinton, W. M., 1961 : Recent Radiometric Studies of the Planets and the Moon. Planets and Satellites, Vol. III, The Solar System, ed. G. P. Kuiper and B. M. Middlehurst, U. of Chicago Press, Chicago, Ill.

20. Murray, B. C., Wildey, R. L., and Westphal, J. A., "Infrared Photometric Mapping of Venus through the 8-14μ Atmosphere Window," J. Geophys. Res. 68(16):4813-4818, August, 1963.

21. Strong, J., Ross, M. D., and Moore, C. B., "Some Observations on the Atmosphere of Venus and the Earth During the Strato Lab IV Balloon Flight," J. Geophys. Res., 65(8):2526, August, 1960.

22. Sagan, C., and Kellogg, W. W., "The Terrestrial Planets," Ann. Rev. Astron. Astrophys. 1:235-266, 1963.

23. Goody, R. M., 1964 : Limb Darkening of Thermal Emission from Venus. Icarus, Vol. 3, p. 98.

24. Chamberlain, J. W., 1965 : The Atmosphere of Venus Near Her Cloud Tops. Astrophys. J., Vol. 141, p. 1184.

REFERENCES (Continued)

25. Sagan, C. and Pollack, J. B., 1965 : Spacecraft Observation of Venus Infrared Limb-Darkening. Annales d'Astrophysique, Vol. 28, p. 229.

26. Kaplan, L. D., 1965 : Remarks on the Mariner 2 Limb-Darkening Measurements. Annales d'Astrophysique, Vol. 28, p. 598.

27. Samuelson, R. E., 1965 : Private communication.

28. Hovis, W. H., 1965 : Unpublished Data.

29. Rea, D. G., 1962 : Molecular Spectroscopy of Planetary Atmospheres. Space Science Reviews, Vol. 1, pp. 159-196.

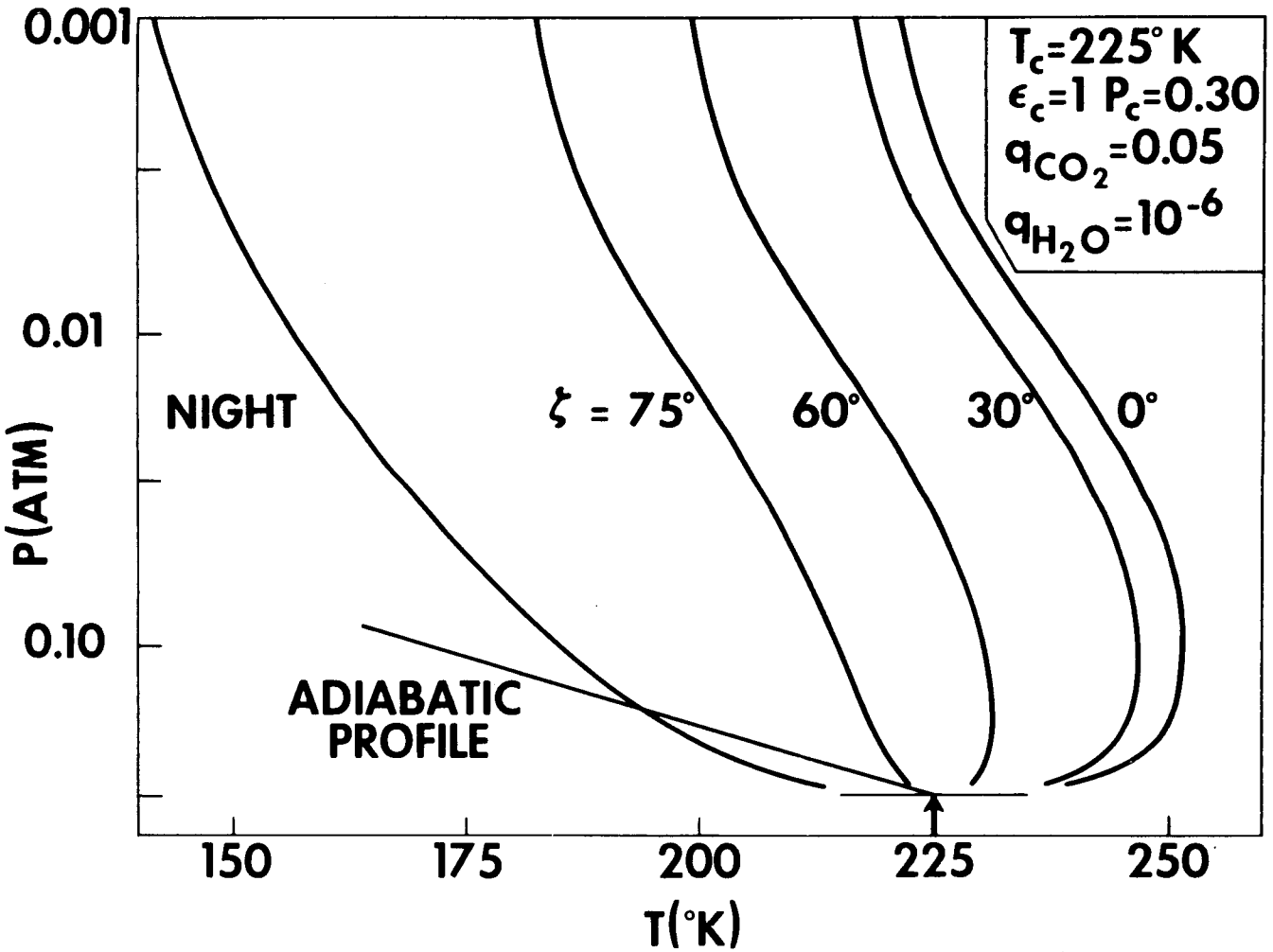

Figure 1—Radiative equilibrium temperatures for several solar zenith angles. Comparison with the adiabatic profile indicates instability for large zenith angles.

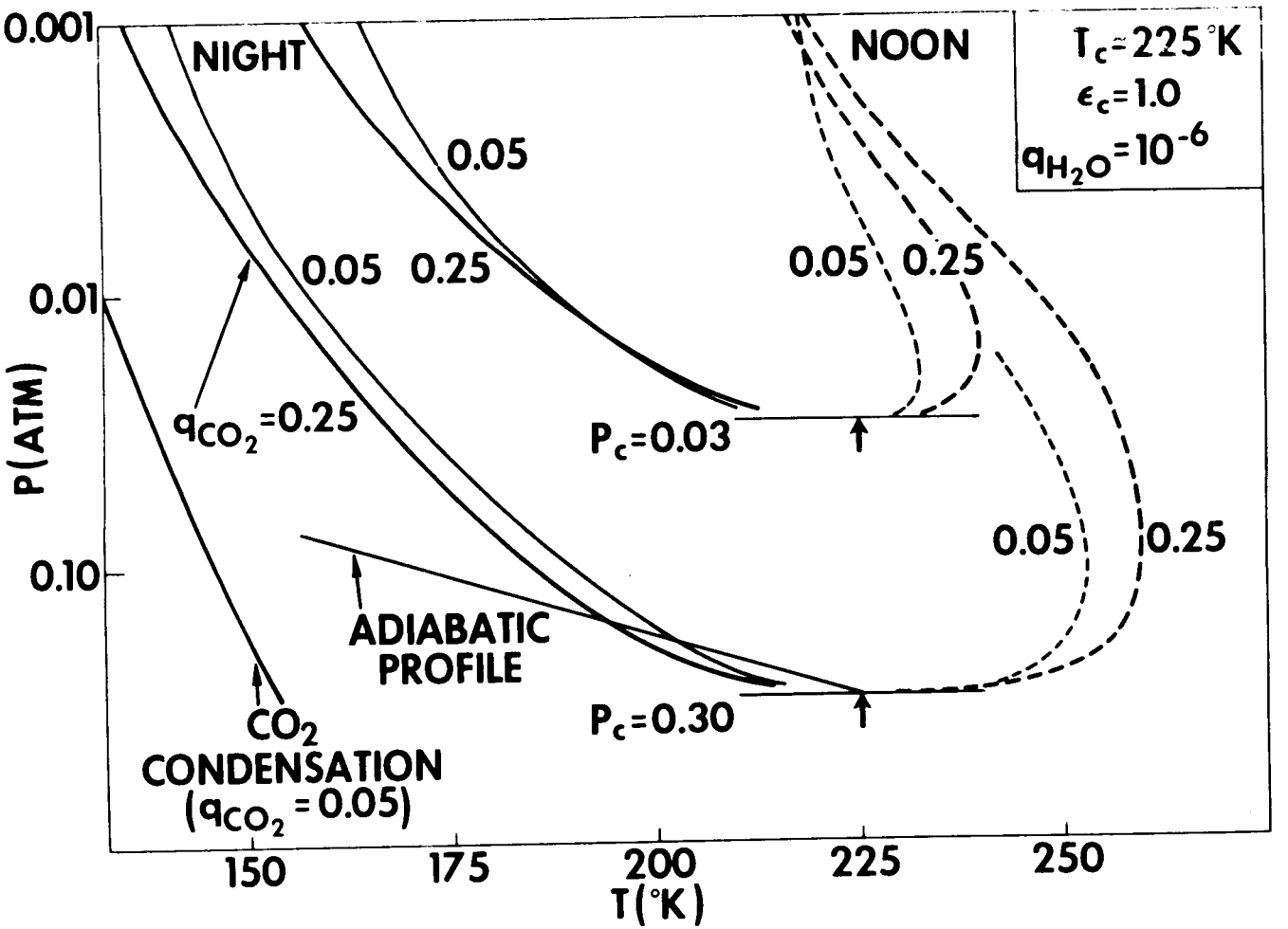

Figure 2—Radiative equilibrium temperatures for both night and day, and for various pressure levels and CO_2 concentrations. Condensation of CO_2 is unlikely for the conditions shown. The adiabatic profile (5% CO_2) is shown.

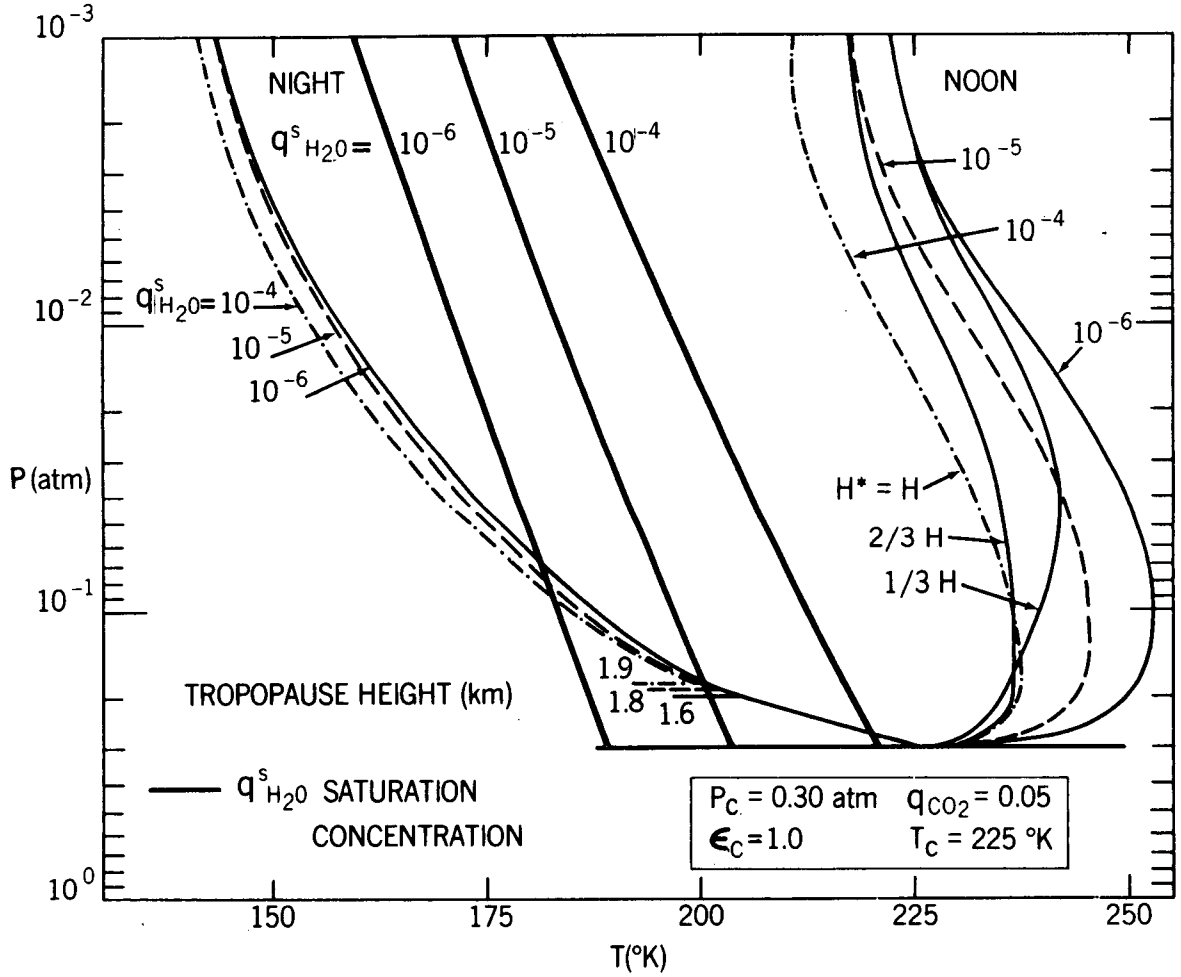

Figure 3—Radiative and convective equilibrium temperatures for several water vapor concentrations and water vapor scale heights. Also indicated are water vapor saturation curves and tropopause heights.

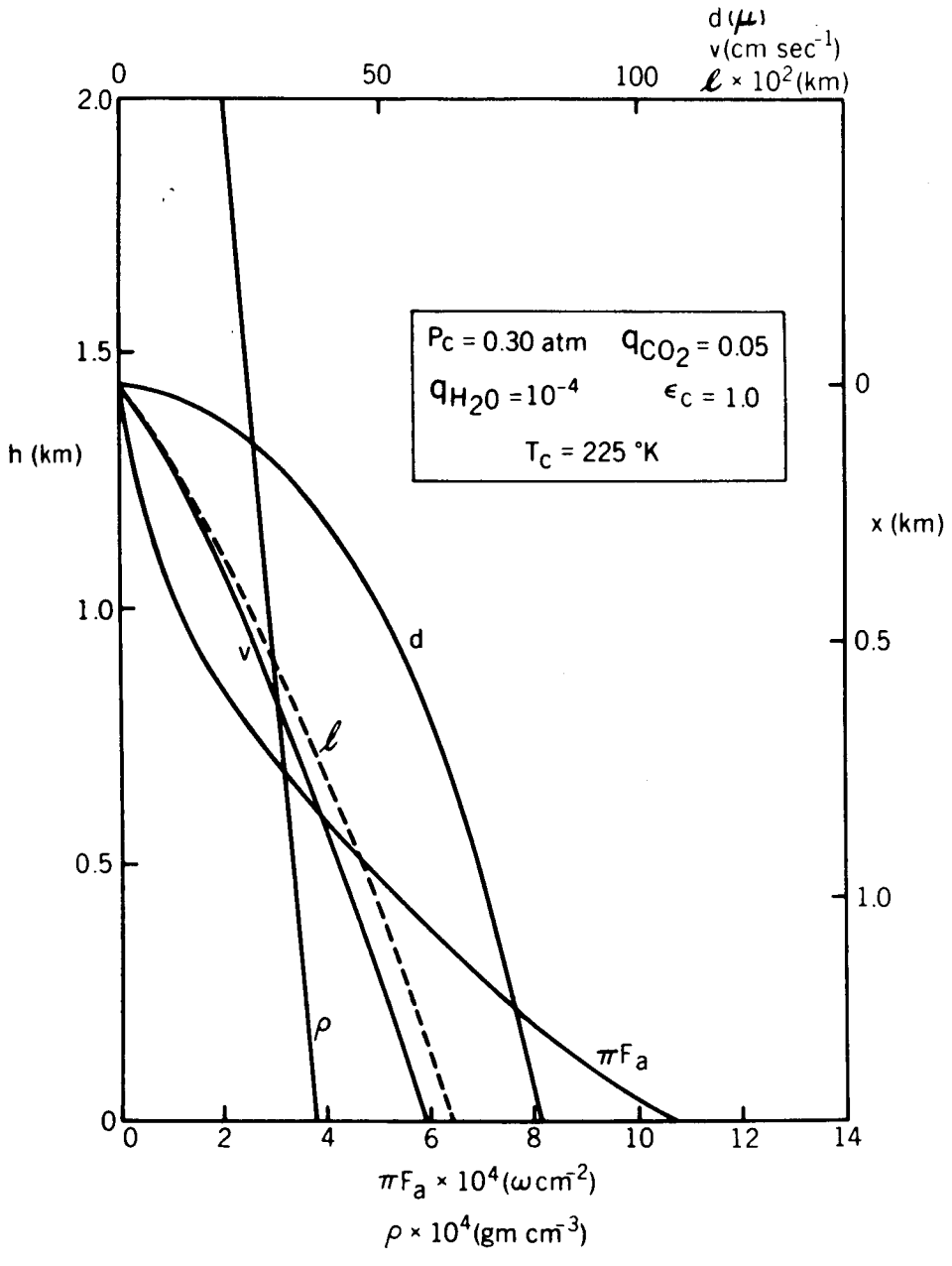

Figure 4—Convective flux, mean vertical gas velocity, mixing length, density and maximum diameter of particles which can be suspended.

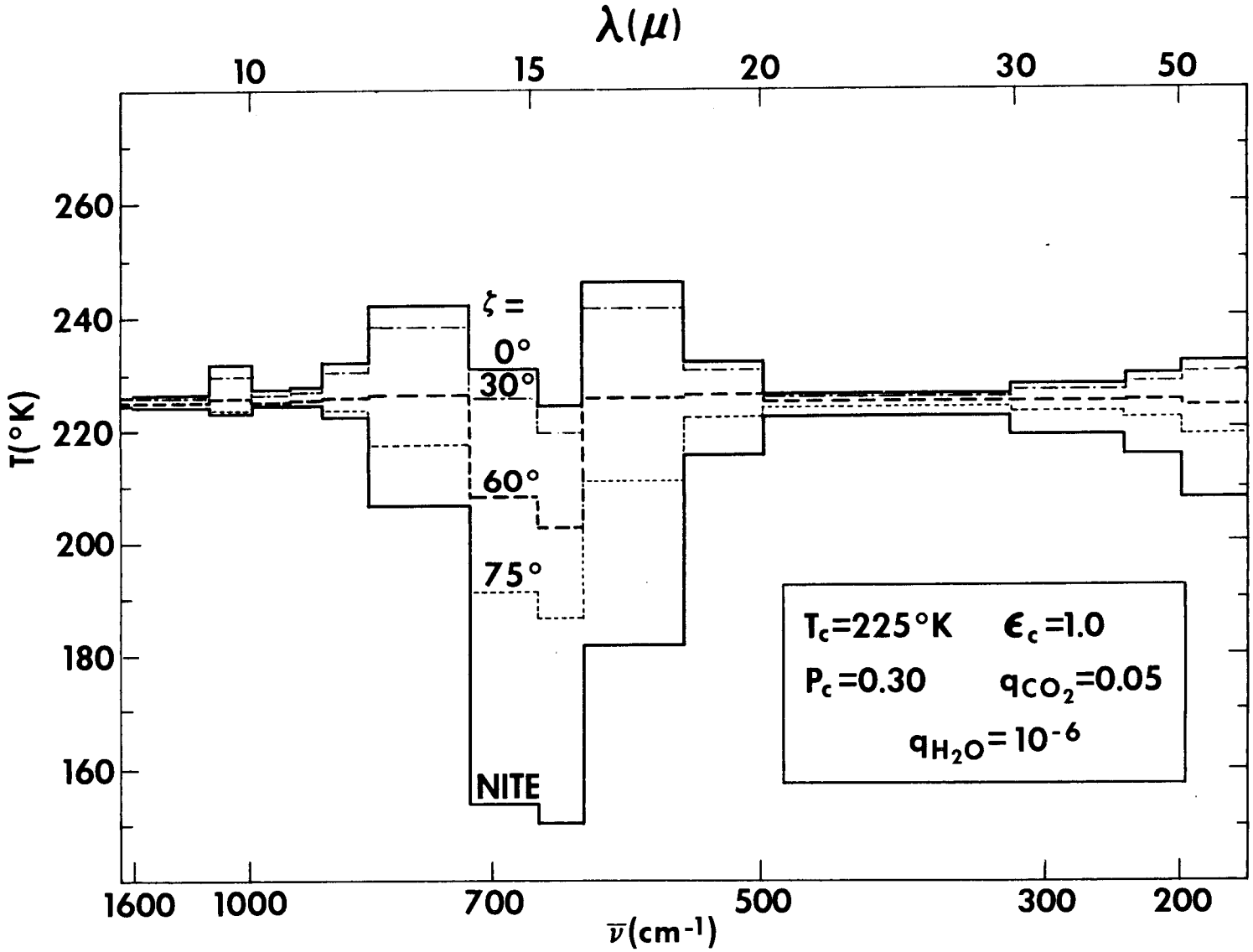

Figure 5—Thermal emission spectra for various solar zenith angles. Brightness temperature is shown as a function of wave-number.

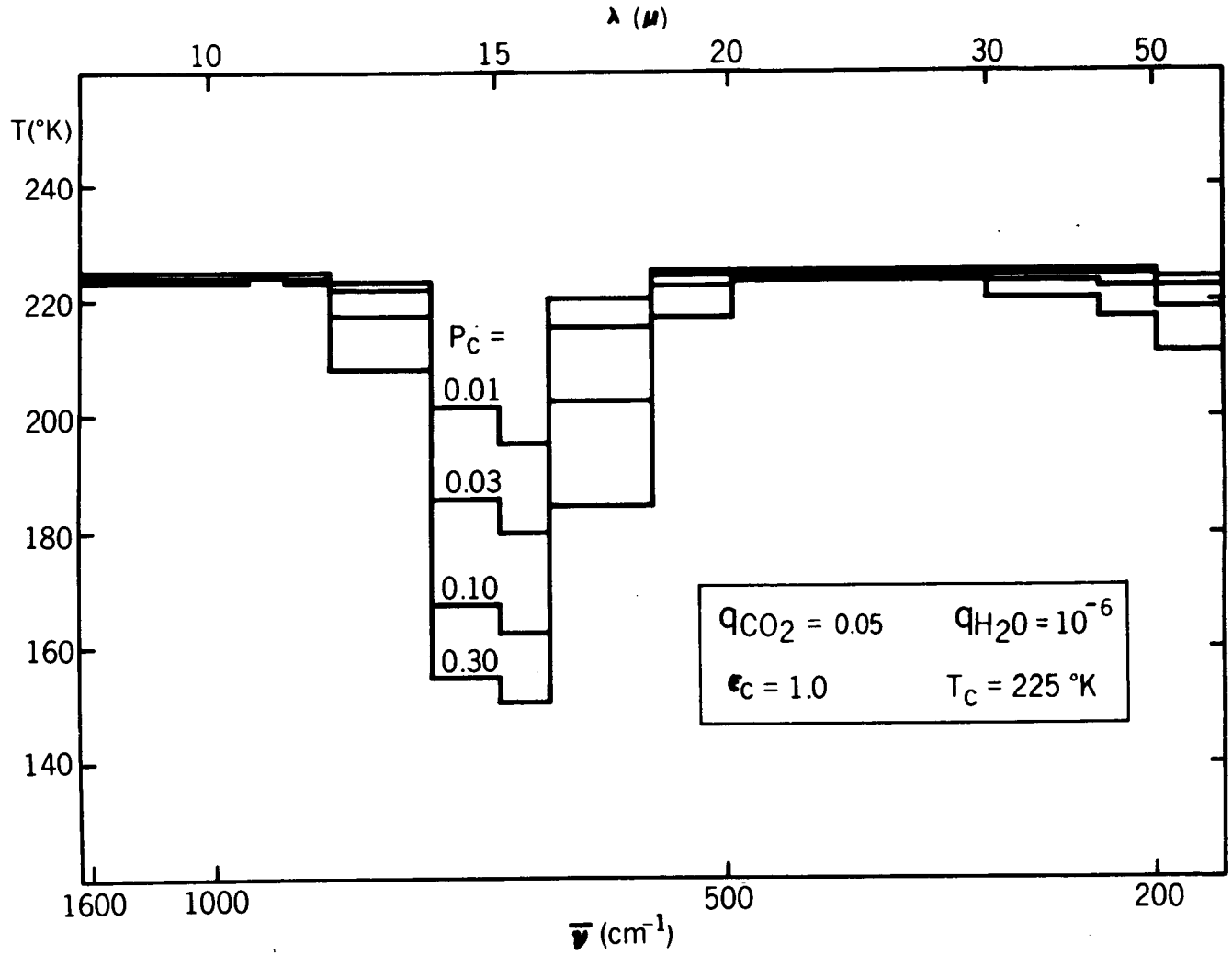

Figure 6—Thermal emission spectra for several cloud top pressure levels in the dark hemisphere.

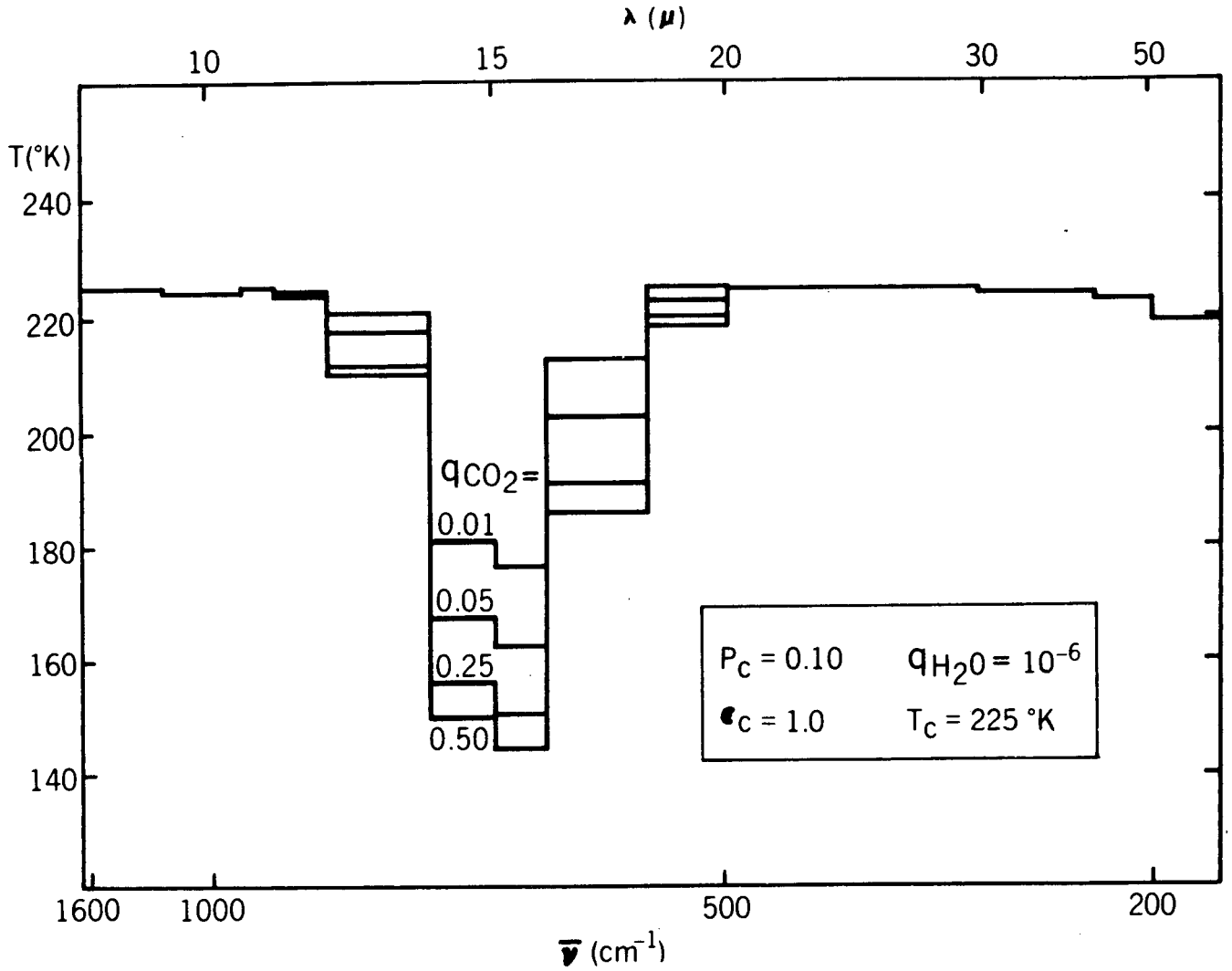

Figure 7—Thermal emission spectra for several CO_2 concentrations in the dark hemisphere.

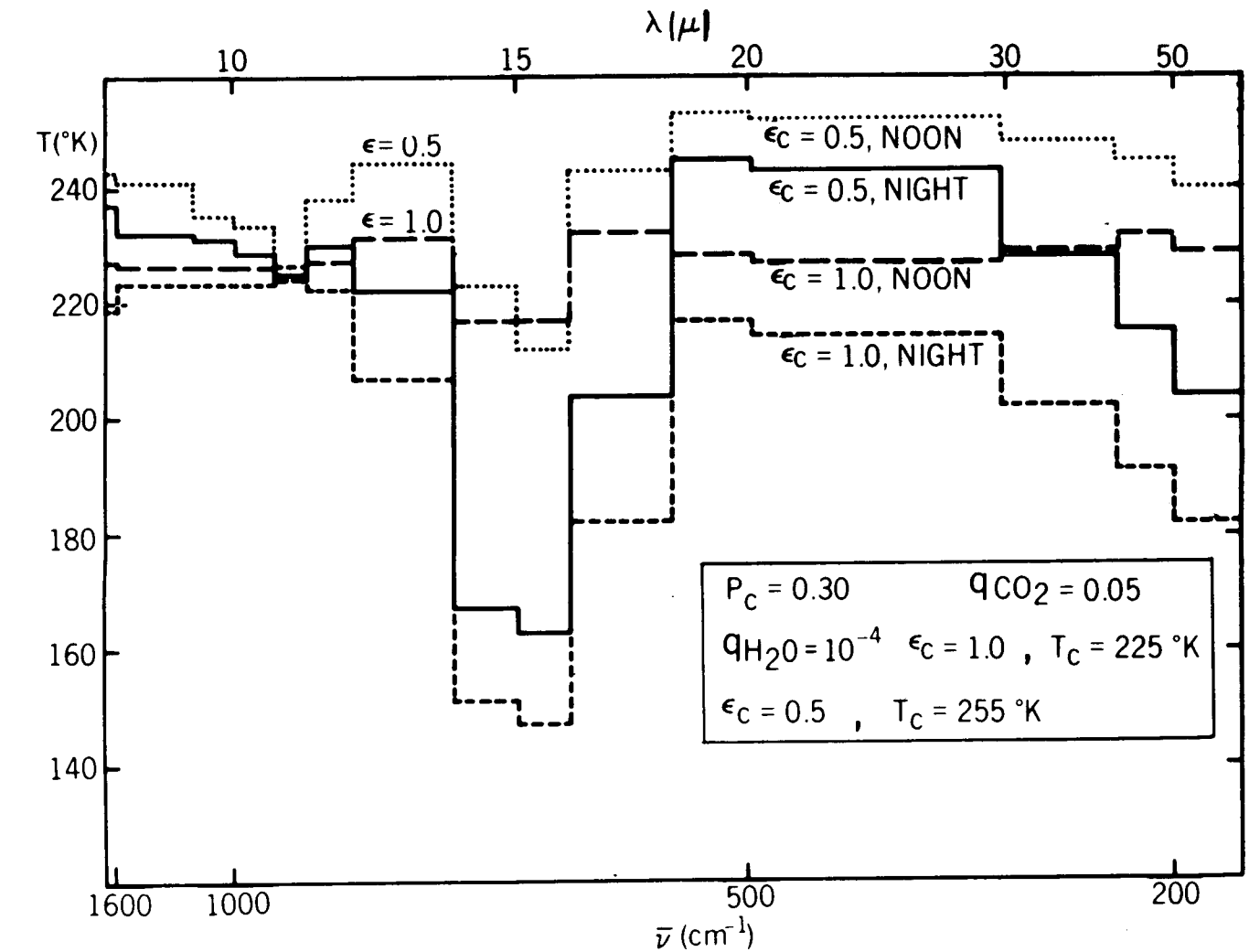

Figure 8—Thermal emission spectra for two cloud emissivities for the dark and the illuminated hemisphere.

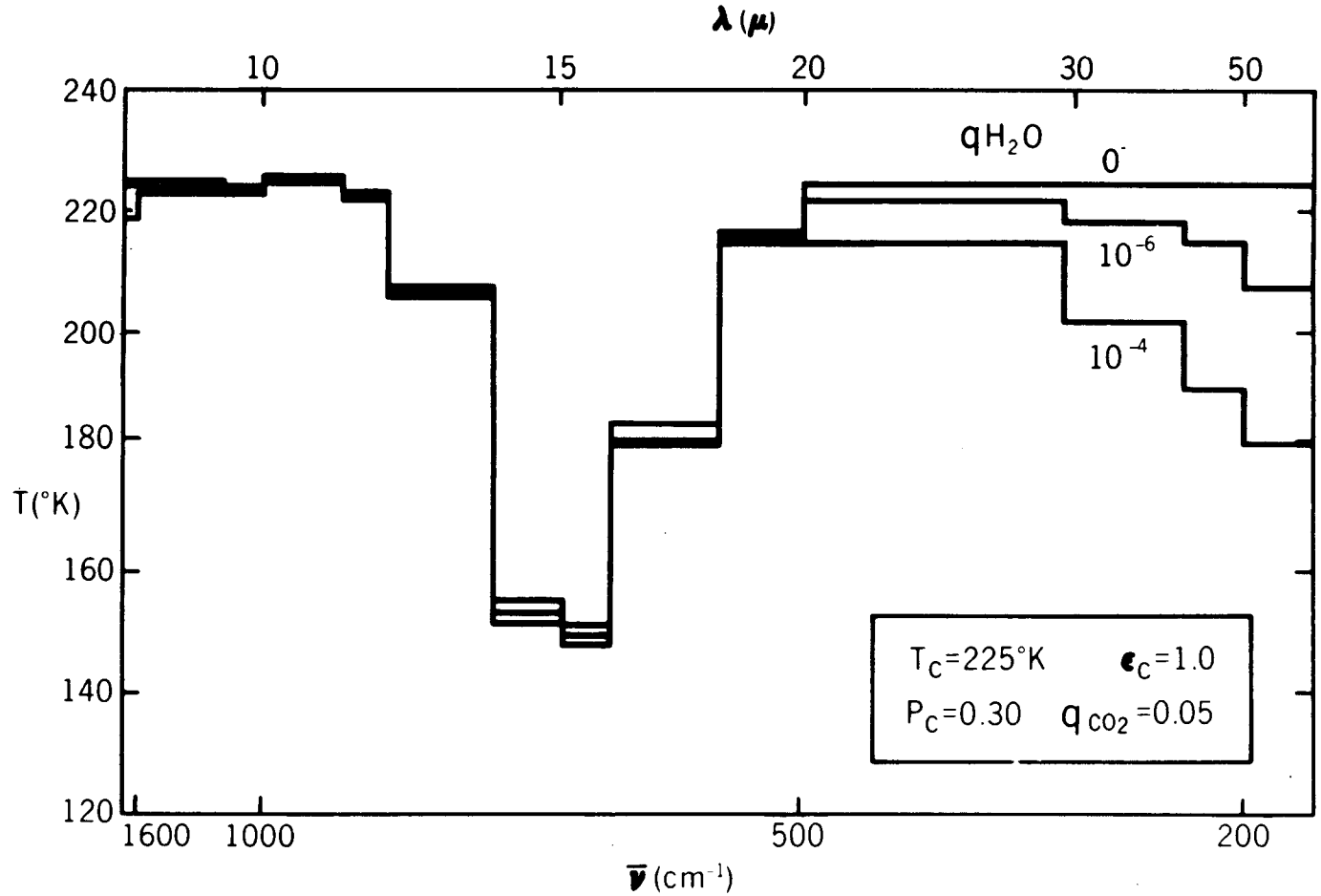

Figure 9—Thermal emission spectra for several water vapor concentrations in the dark hemisphere.

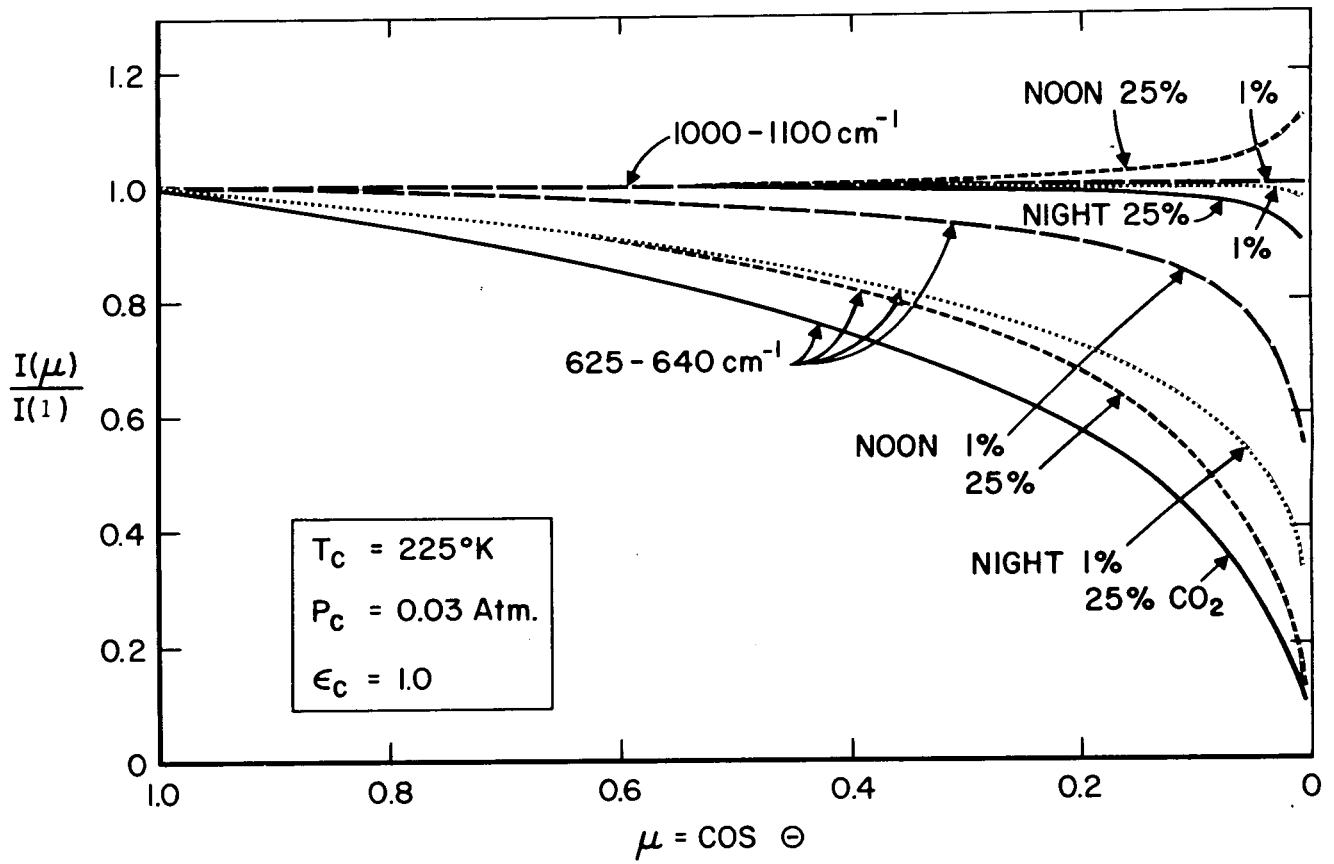

Figure 10—Planetary limb functions in a weakly and a strongly absorbing spectral interval. Various CO_2 concentrations are shown for both hemispheres.

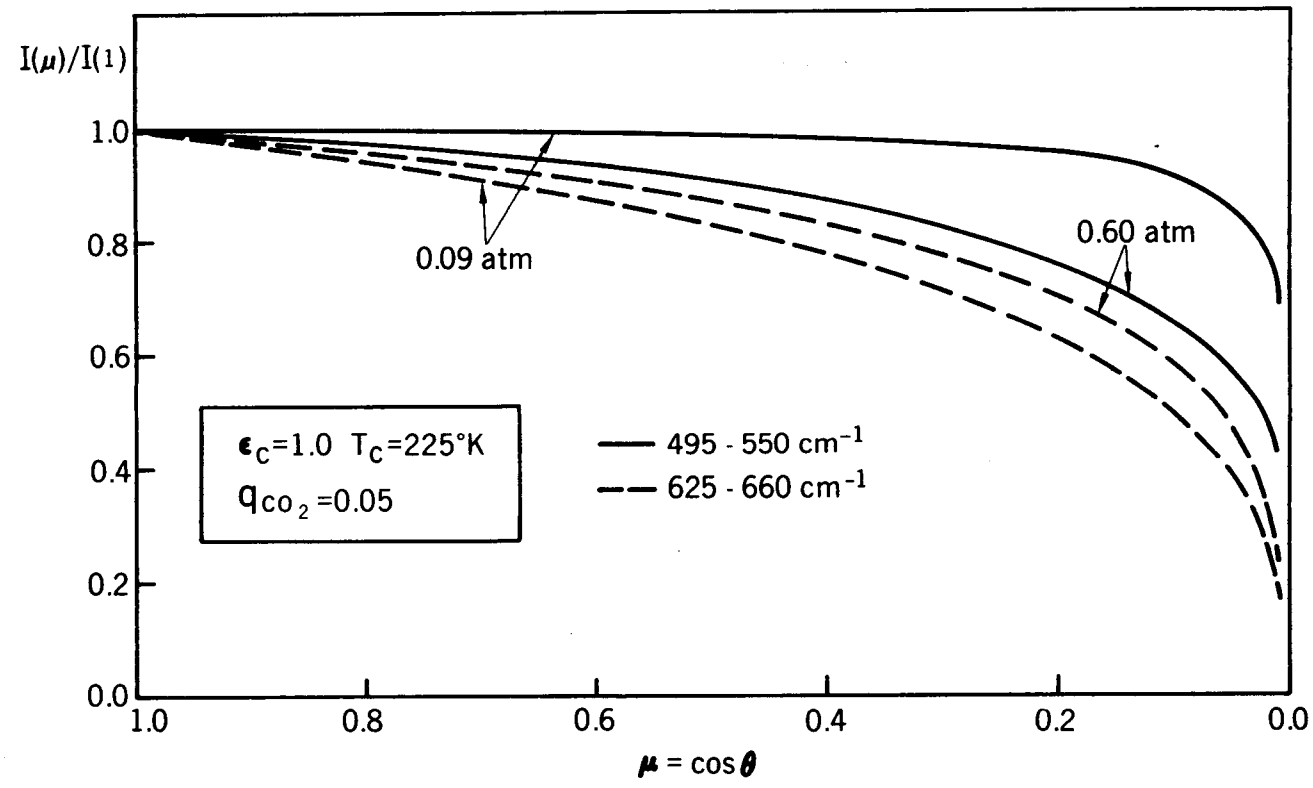

Figure 11—Planetary limb functions for a weakly and a strongly absorbing spectral interval for two cloud top pressure levels.

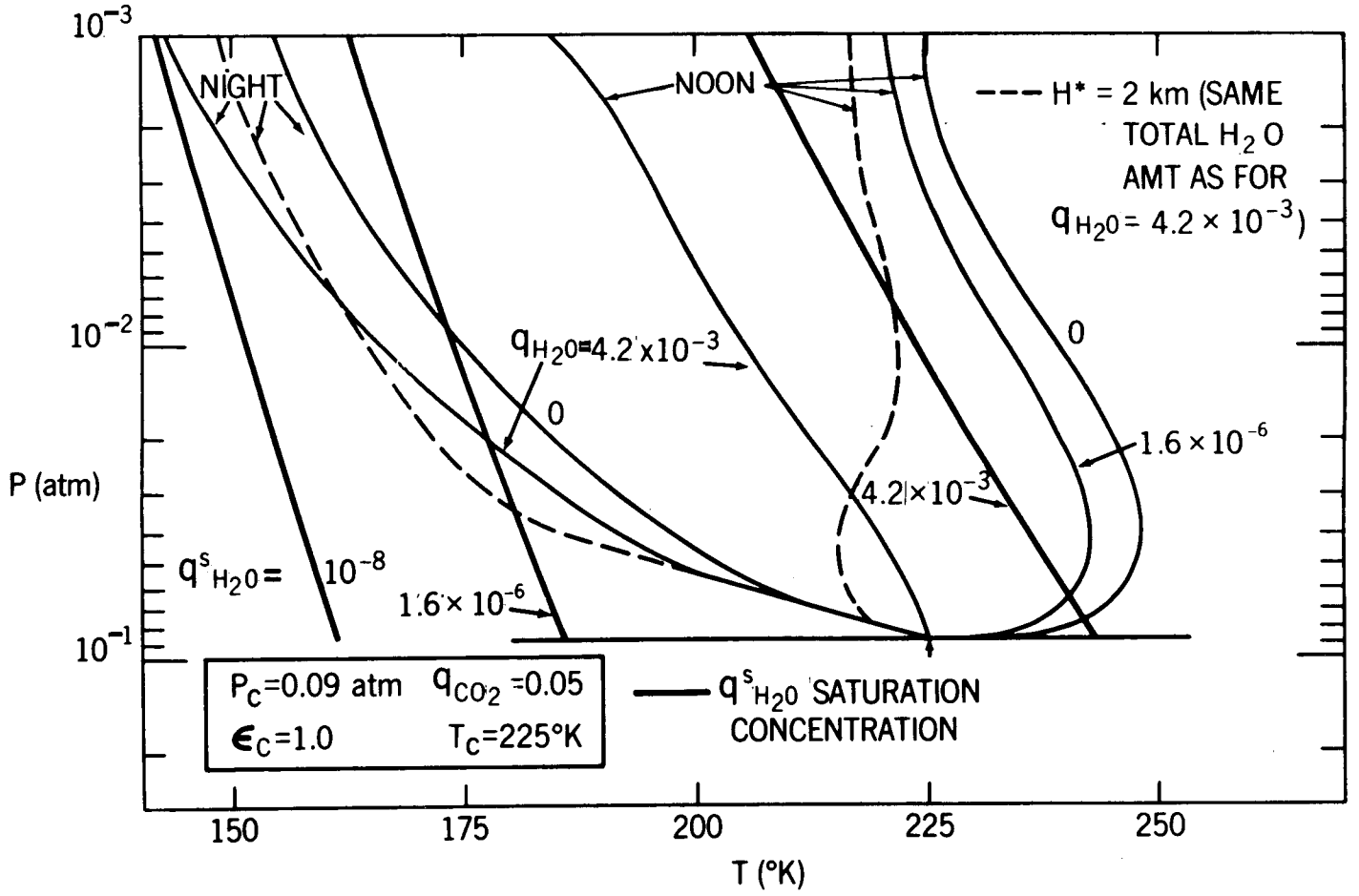

Figure 12—Equilibrium temperatures for an .09 atm cloud top pressure, emissivity of one, and water vapor concentrations corresponding to the data of Bottema, Plummer and Strong as well as to the data of Spinrad.

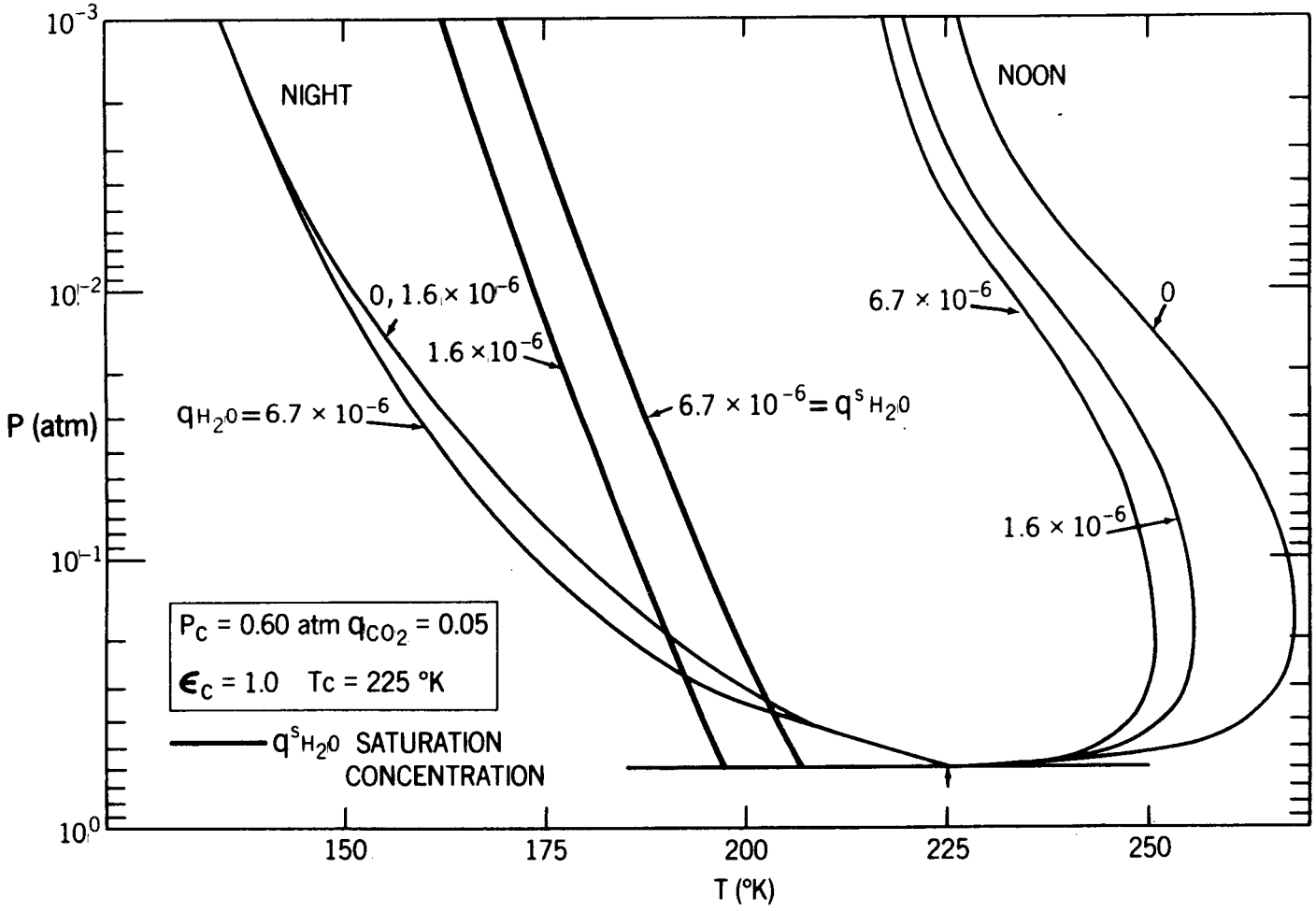

Figure 13—Equilibrium temperatures for an 0.6 atm cloud top pressure, emissivity of one, and several observed water vapor concentrations.

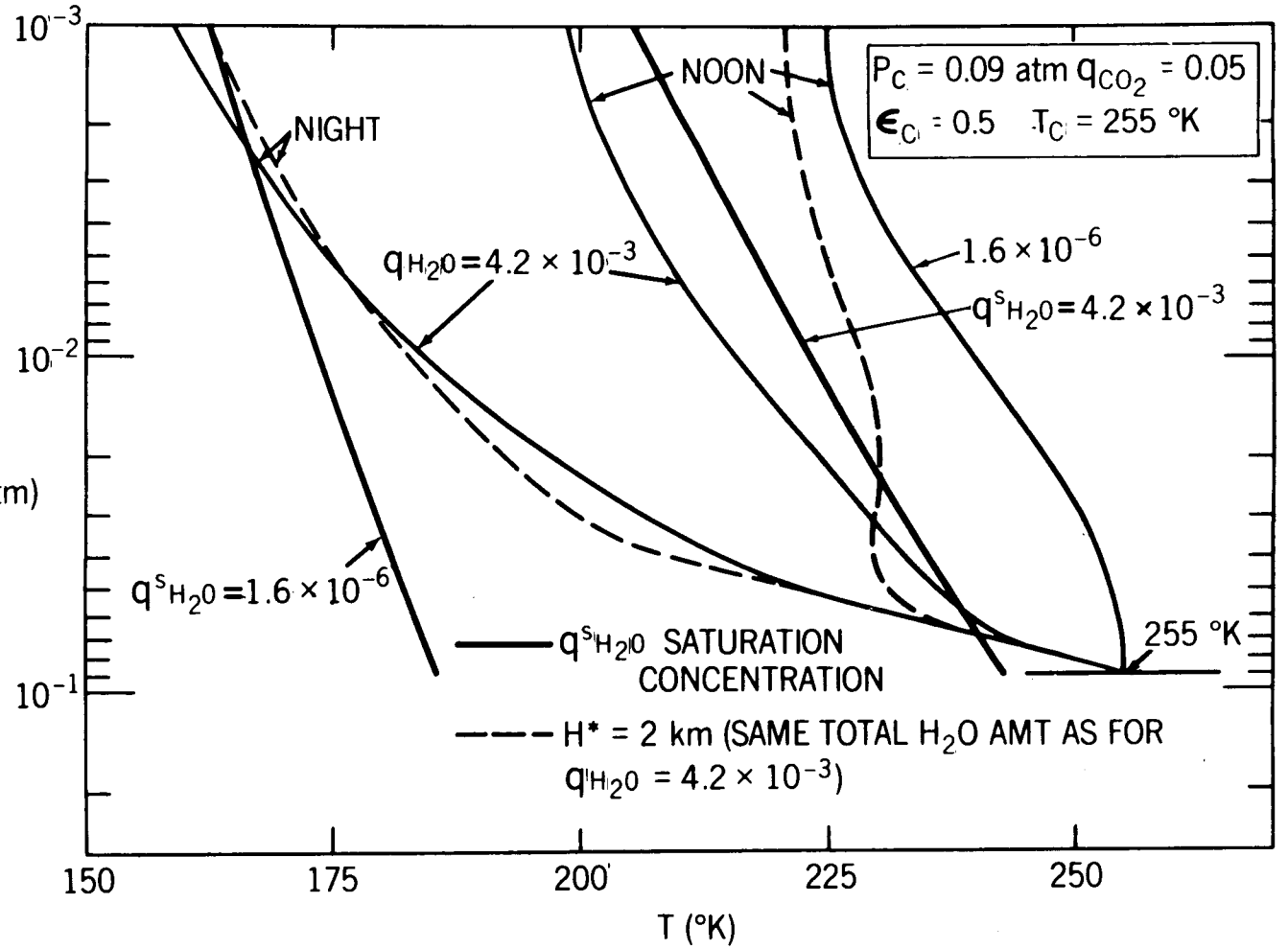

Figure 14—Equilibrium temperatures for a .09 atm cloud top pressure, emissivity of 0.5, and several observed water vapor concentrations.

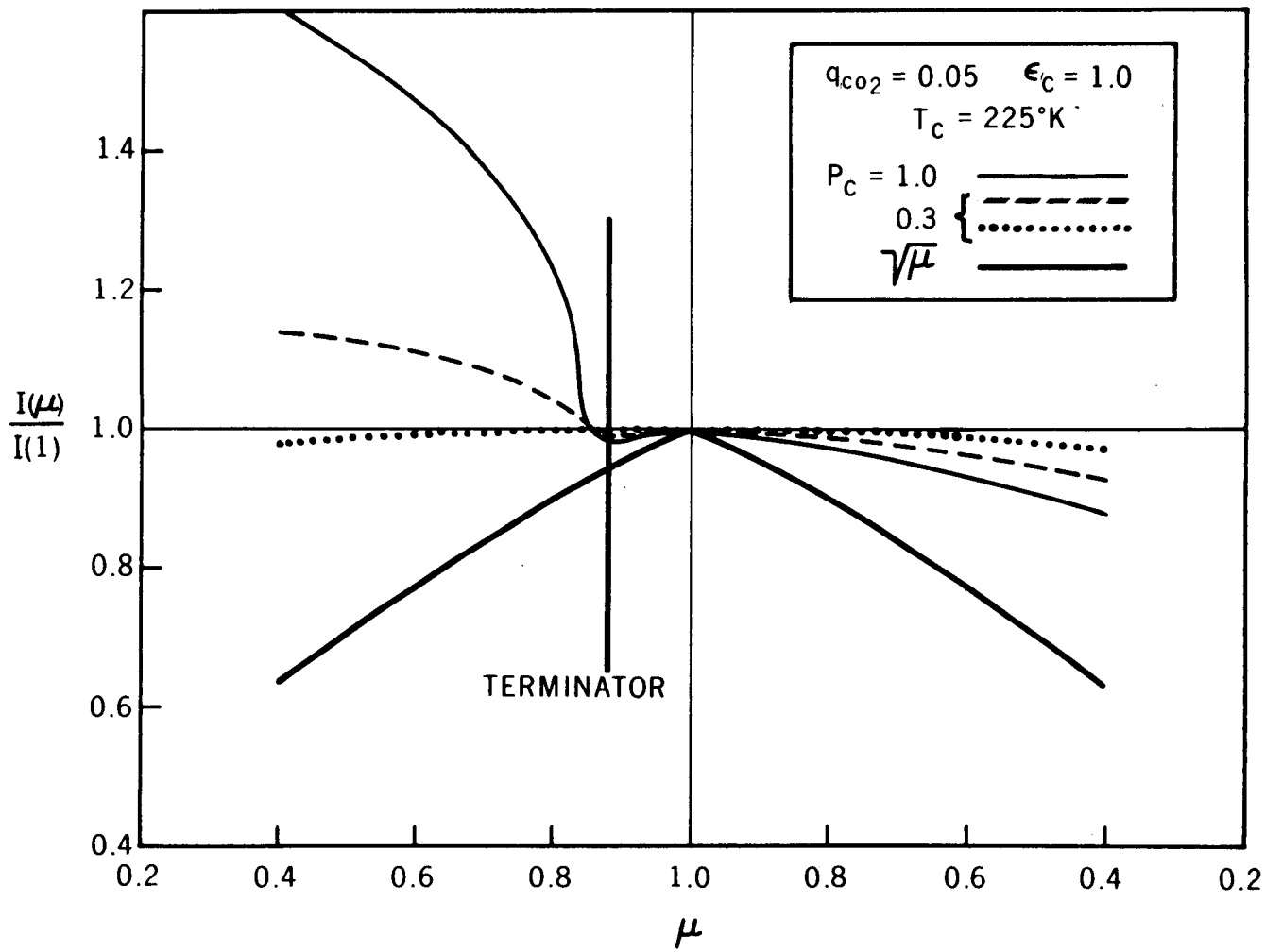

Figure 15—Comparison of computed limb functions with planetary observations. Several pressures and water vapor concentrations are shown.

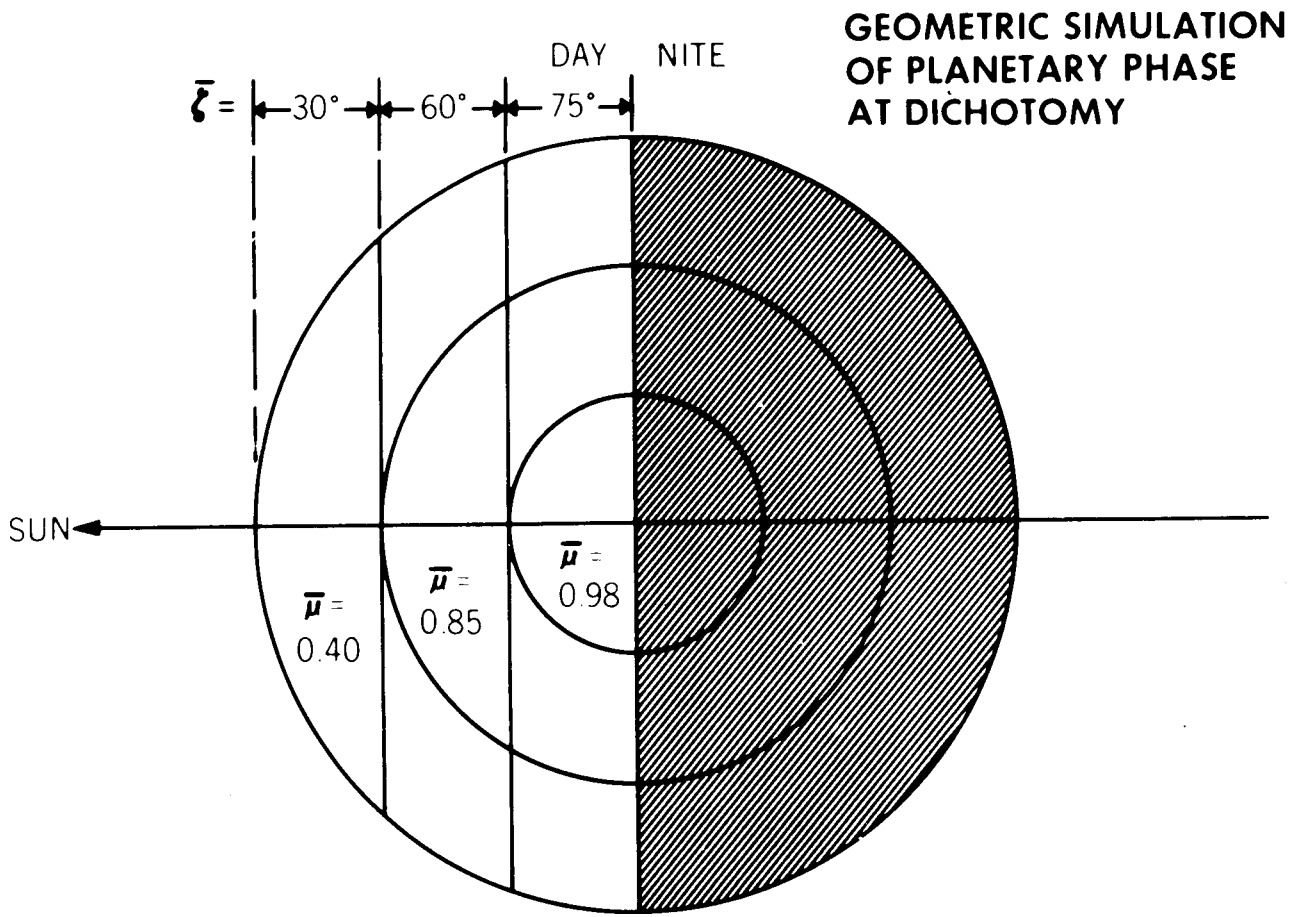

Figure 16—Relative area weighting functions applied to the specific intensity to simulate measurements of planetary spectra.

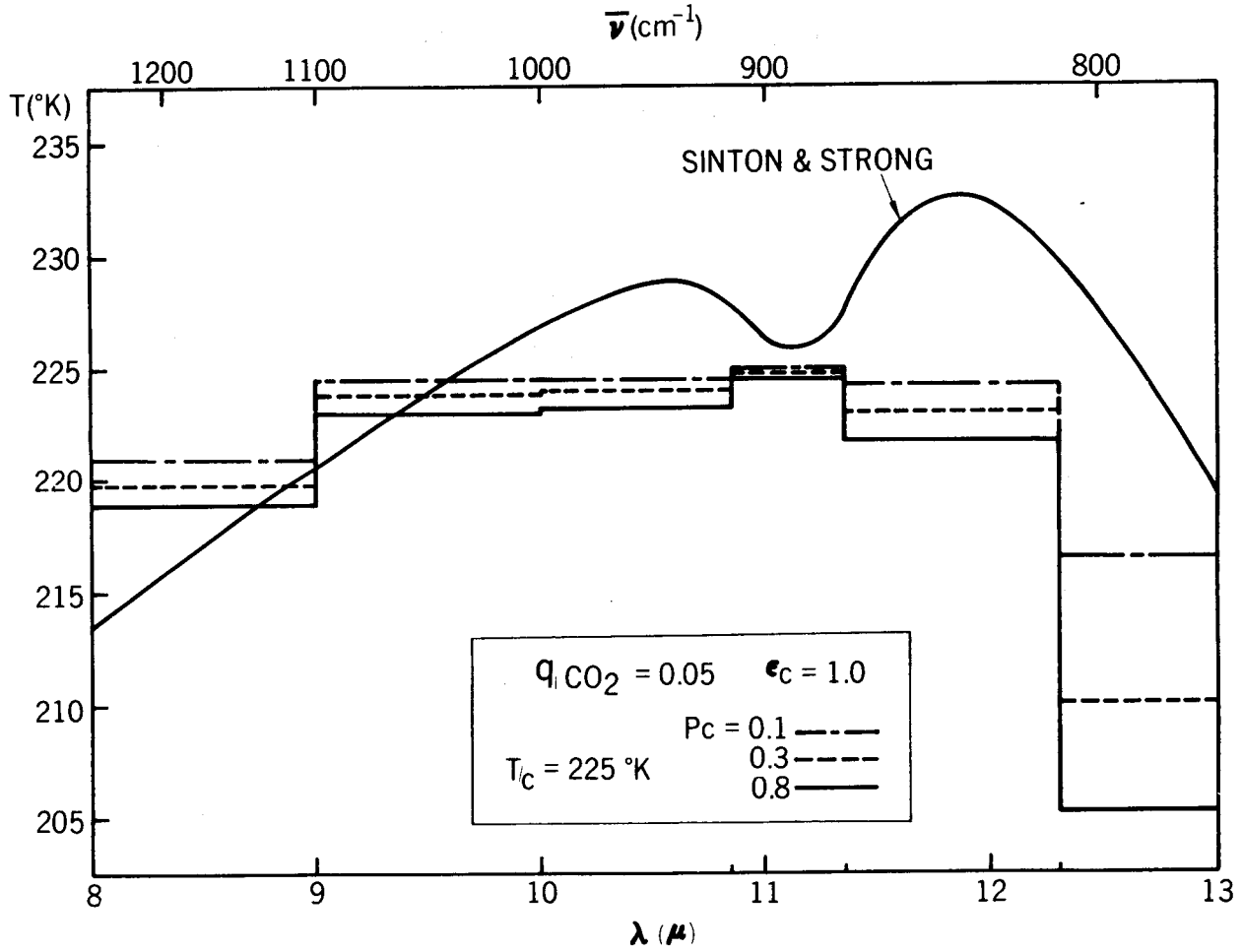

Figure 17—Synthesized spectra in the 8-13μ window for several cloud top pressures and the observed spectrum of Sinton and Strong.

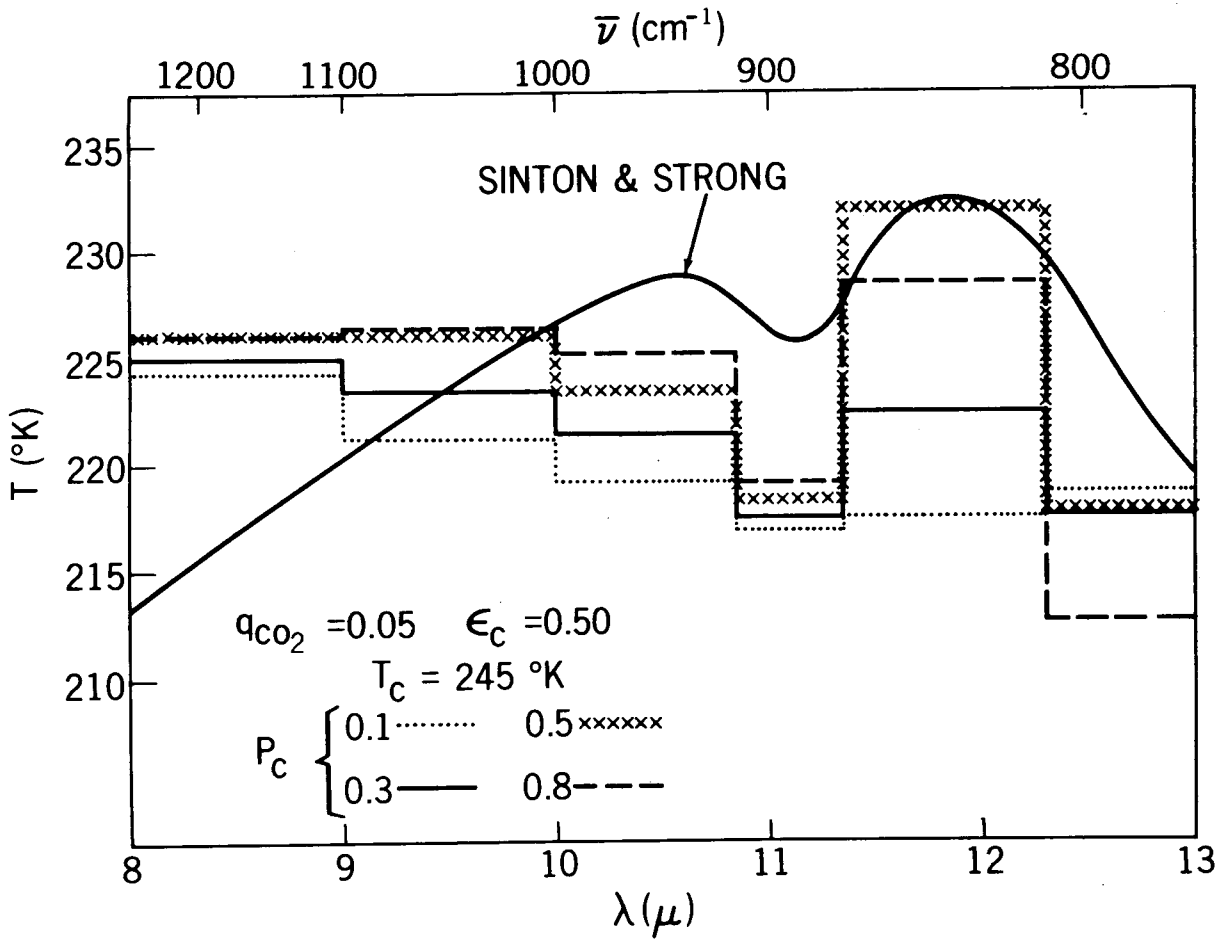

Figure 18—Synthesized spectra in the 8-13μ window for several cloud top pressures.